Summer 2021

Protection of modern distribution systems

Fahd Amin Hariri

Department: Electrical and Computer Engineering

PROTECTION OF MODERN DISTRIBUTION SYSTEMS

by

FAHD AMIN HARIRI

A DISSERTATION

Presented to the Graduate Faculty of the

MISSOURI UNIVERSITY OF SCIENCE AND TECHNOLOGY

In Partial Fulfillment of the Requirements for the Degree

DOCTOR OF PHILOSOPHY

in

ELECTRICAL ENGINEERING

2021

Approved by

Mariesa L. Crow, Advisor
Mehdi Ferdowsi
Pourya Shamsi
Rui Bo
Suzanna Long

PUBLICATION DISSERTATION OPTION

This dissertation consists of the following three articles, formatted in the style used by the Missouri University of Science and Technology:

Paper I: New Infeed Correction Methods for Distance Protection in Distribution Systems. Pages 3-39 have been submitted to Energies.

Paper II: A New Approach to Protection Coordination for Distribution Systems with Distributed Generation. Pages 40-61 have been submitted to Electric Power Components and Systems-Taylor & Francis.

Paper III: Modeling and Simulation of Resistive Superconducting Fault Current Limiter in PSCAD™/EMTDC™. Pages 62-80 have been submitted to North American Power Symposium (NAPS).

ABSTRACT

Motivated by the potential for improvements in the electric distribution system's protection schemes, this work examined the challenges facing protection schemes due to the integration of Distributed Generators (DGs). Traditional protection schemes for radial distribution systems were designed based on the unidirectional power flow from the source down to the loads. Protective devices typically use are overcurrent relays, autoreclosers, fuses, and circuit breakers. However, these protective schemes may no longer be sufficient to ensure correct operation in the new era of distribution systems integrated by DGs. This research investigated the impact of DGs that might mislead the protection schemes in distribution systems. Understanding these impacts are helpful for improving protection schemes solution methodologies.

This work also presented multiple solutions for protection schemes aimed at mitigating the negative impacts of integrating DGs into radial distribution systems. The first proposed solution provided improvements for distance relays (DRs) that were proposed recently to protect radial distribution feeders (RDFs). This solution consisted of three new methods to accurately calculate the measured positive-sequence impedance by DR in the presence of the infeed effect. These methods depended only on local measurements making them cost-effective and easy to implement compared to other solutions that depend on communication links.

The second solution proposed a new approach to control inverter-based DGs (IB-DGs). This approach limited the fault current in distribution systems by controlling single-phase inverters that connect distributed generators to distribution systems. Finally, this research proposed an accurate and reliable model for the resistive superconducting fault current limiter (SFCL). The performances of the proposed methods were demonstrated with radial distribution system models in PSCAD™/EMTDC™.

ACKNOWLEDGMENTS

First and foremost, I thank the Almighty for his generosity and kindness all these years. I was able to reach this stage of my life because of his blessings.

I express my sincere gratitude to my advisor Dr. Mariesa Crow for the continuous support of my Ph.D studies and related research, for her patience, motivation, and immense knowledge. Her guidance helped me in research and write this dissertation. I am also very grateful for the assistance and advice provided by my doctoral committee members: Dr. Mehdi Ferdowsi, Dr. Pourya Shamsi, Dr. Rui Bo, and Dr. Suzanna Long. Their comments greatly influenced my understanding, which allowed me to achieve the desired results.

I express my deepest gratitude for my father, Amin Hariri, for his constant support and faithful prayers during my academic studies. I dedicate this dissertation to my late mother, Raja Hajjar, who always believed in my ability to be successful in the academic arena. You are gone, but your belief in me made this journey possible. I can never thank my parents enough for their encouragement and love.

I greatly appreciate the companionship and patience of my wife, Afnan Hilal. Her support throughout my graduate studies was essential to my success. It would never have been done without her encouragement and support.

I cannot forget to thank my daughters Raja, Alyaa, and Malak, and my son Naif—for their love, company, understanding, and encouragement.

Finally, I express my special appreciation and thanks to my country, the Kingdom of Saudi Arabia, and King Abdulaziz University for giving me this valuable opportunity to complete my graduate studies.

TABLE OF CONTENTS

LIST OF ILLUSTRATIONS

Figure Page

PAPER I

PAPER III

LIST OF TABLES

SECTION

1. INTRODUCTION

Electric energy is essential for the progress and development of societies. All residential, commercial, and industrial facilities depend on electric power. Therefore, electric power must be available continuously and reliably. Building new power plants or expanding existing ones is a costly solution to meet increasing annual demands for electric power. By contrast, Distributed Generators (DGs) are considered one of the most promising solutions to meet growing energy demands. At the distribution system (DS) level, DGs are deployed in multiple locations, especially near loads. Therefore, it is characterized by low active power losses resulting from the transmission of energy through transmission lines and feeders over long distances. The power capacities of DGs connected to DS are small (ranging from 100 kW - 10 MW) compared to conventional generation stations.

The DGs were distinguished by the fact that some of them depend on renewable energy, such as solar and wind. With the development of technologies used for renewable energy, the spread of DGs is appropriate in terms of economic returns. By contrast, the integration of DGs into the DSs creates new challenges for the protection system. For instance, the Distance Relay (DR) does not see the actual positive-sequence impedance due to the infeed effect caused by one or more DGs between the main source and the fault location. The infeed effect causes the impedance seen by the relay to be larger than the actual positive-sequence impedance between the relay and the fault point, so the relay is underreached.

Moreover, the fuse-saving scheme to protect overhead lines in DSs was designed based on the one-way flow of energy from the substation to the loads. The presence of DGs in the DSs impact the protection coordination between the fuse and the recloser due to the difference in the amount of fault current passing through each of them during faults. Also, the presence of DGs converts the DSs from a passive network to an active network, in which energy flows in both directions (i.e., from the substation to the loads side and vice versa).

This dissertation proposed different solution methodologies to address the aforementioned issues in DSs. These solutions were proposed in three papers. Paper I proposed new methods to estimate the distance to the fault in the presence of infeed effects in the radial distribution feeder or transmission line. Paper II proposed a new approach to maintain the fuse-saving scheme in DS by controlling the output current of the Inverter-Based DG (IBDG). Finally, a reliable and accurate model of a resistive superconducting fault current limiter (SFCL) was proposed in paper III.

PAPER

I. NEW INFEED CORRECTION METHODS FOR DISTANCE PROTECTION IN DISTRIBUTION SYSTEMS

Fahd A. Hariri, and Mariesa L. Crow
Department of Electrical & and Computer Engineering
Missouri University of Science and Technology
Rolla, Missouri 65409–0050
Email: fahrz9@mst.edu

ABSTRACT

The reliability and security of power systems may be jeopardized by the increase in the amounts of renewable generation and the uncertainties produced by these devices. In particular, the protection schemes of traditional power systems have been challenged by the integration of distributed generation (DG) resources. Distance relays (DRs), which have been mainly employed to protect transmission systems, are increasingly proposed as one of the solutions to protect distribution systems with a heavy penetration of DGs. However, conventional distance protection faces several drawbacks that might lead to maloperation. One of those challenges is the "infeed effect", which causes the impedance seen by the distance relay to be larger than the actual positive-sequence line impedance between the fault and relay location. This paper proposes three new methods to estimate the distance to the fault in the presence of infeeds, whether in a radial distribution feeder or transmission line. Unlike other solution methodologies in the literature that require communication links to estimate the distance to the fault, the proposed methods only need the local measurement (i.e., the voltage and current measurements at the location of distance relay) to do the same. The performance of the method is demonstrated with a radial distribution system model in PSCAD™/EMTDC™.

1. INTRODUCTION

As opposed to traditional distribution systems (DS) in which the substation is the primary source of generation, the integration of distributed generation (DG) brings generation closer to consumers by siting generation along the feeder. DG is typically considered to be one of the following energy sources: photovoltaics (PV), small wind turbines, diesel generators, batteries, hydroelectric generators, or micro-turbines [1]. Siting small to medium power generating stations closer to the customer reduces overall energy consumption by decreasing active power losses incurred during the transmission of electricity, thereby reducing reliance on fossil fuels and improving environmental concerns. In addition, the deployment of more efficient DG-based systems reduces economic costs and aids in development of renewable energy. Also, integration of DG-based sources improve the operational reliability in the load centers that are remotely connected to the primary power grid and overloaded urban zones. While there are many advantages to integrating DG into the DS, the presence of DGs may complicate the existing protection of DSs, which are usually protected with overcurrent protection equipment such as overcurrent relays (OCRs) and/or fuses.

With the predominant DGs integration, the traditional radial and unidirectional single source-based distribution system configuration is changed into bidirectional, multi source-based distribution system [2]. Examples of the influences of DG on current protection are shown in Figure 1. At the inception of the fault, as shown in Figure 1a, the distribution substation and the DG jointly provide the fault current to the fault point. The DG fault current contribution increases the fault current. In Figure 1a the CB1 should isolate the fault and CB2 must not operate. However, the high fault current may cause maloperation of both breakers (i.e., CB1 and CB2). The maloperation of CB2 will cause a power outage to all customers connected to the healthy feeder (i.e., the unfaulted feeder). If a fault occurs downstream of the DG, as shown in Figure 1b, the fault current consists of the fault current contribution from the DG and the fault current from the distribution

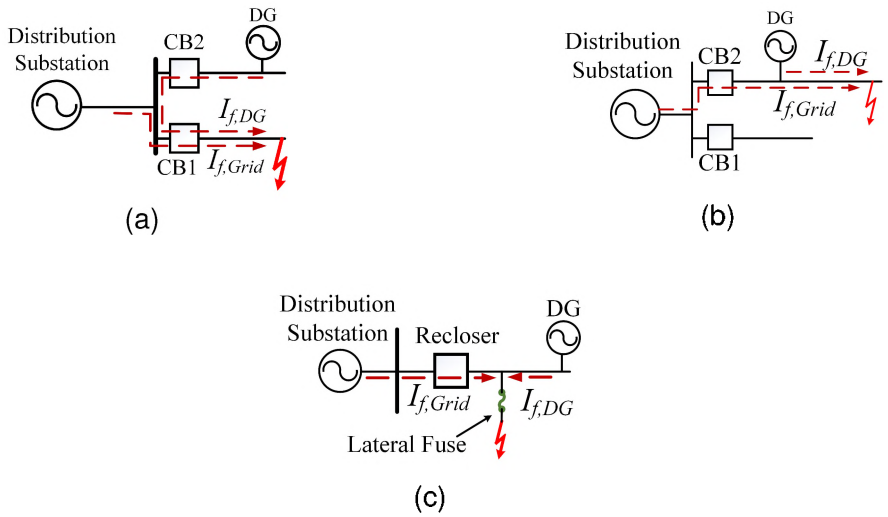

Figure 1. Fault current contributions for (a) a fault on a neighboring feeder, (b) a downstream fault, and (c) a fault on a lateral feeder.

substation. Thus, DG in Figure 1b decreases the fault current through CB2 compared to the case with no DG. This situation could cause "fail-to-trip" of CB2 because the overcurrent protection sees a lower fault current than its trip settings.

The integration of DG on a distribution feeder, as shown in Figure 1c will affect the coordination between the recloser and fuse. If a fault occurs, the fault current passing through the recloser would be lower than the fault current if there were no DG in the system. At the same time, the current through the fuse consists of the currents from the distribution substation as well as the current from the DG, which means that the fuse current is no longer the same as the current passing through the recloser. As a result, recloser-fuse coordination may be lost. Therefore, the protection philosophy of distribution systems must be reviewed and developed to overcome the new challenges posed by the integration of DG. Protection challenges due to such situations and corresponding solutions are discussed in [3–5]. One of the solutions that provides a reliable and secure protection scheme for DG-integrated DS is using distance relays (DR) in place of overcurrent relays [6].

DRs which are used mainly to protect transmission systems in the past, have been proposed as one of the potential solutions to protect radial distribution systems [7, 8]. The significant advantages of DR which include its innate ability to detect faults in both directions (depending on the characteristics of the DR), and ; free from external system factors. These features make DR an favorable choice for distribution system protection in comparison to overcurrent protection [6]. However, integrating DGs in radial distribution system may create issues that affect the reliability and sensitivity of DRs. Some of these issues include the proper setting of the zero-sequence compensation factor K_0, the fault resistance, and the infeed effect [9–11].

The infeed effect due to the integration of DGs in radial distribution systems causes the impedance seen by the relay to be larger than the actual positive-sequence impedance between the relay location and the fault position, causing the relay to underreach [12]. Changing the DR settings to protect a line in a distribution system equipped with one or more DGs often results in large settings. In other words, to address the infeed effect the DR impedance settings would be increased. However, these large settings may causes maloperation of the DR during system disturbances, especially in heavy-load periods or during stable swing oscillations [12].

One solution that has been used in transmission lines to solve this problem are intertripping schemes, such as underreach with direct tripping, permissive underreach intertripping, and permissive overreach intertripping [13, pp. 210–213]. These communication-based schemes have been proved to be a very reliable solution. Another communication-based solution that has been proposed in [14] uses the real-time measurements of the current at various locations to compensate for the impedance calculated by the DR. However, these schemes have the disadvantage that they explicitly rely on a communication network, therefore if the communication system fails (either by natural or cyber interference) the result will be miscoordination of the protection system. Moreover, comparing currents at line

ends is expensive as it requires communication circuits to be at least as long as the lines themselves to be protected. Furthermore, the maintenance cost of these communication systems can be significant [15]. In the remainder of this paper, we propose several methods that avoid the disadvantages posed by the communication requirement.

The objective of this paper is to introduce an accurate and inexpensive approach to mitigate the infeed effect. The proposed approach is a cost-effective solution since it just requires only the measurements at the relay location to estimate the distance from the DR location to the fault location in the presence of one or more distributed power sources. Hence, there is no need to install any additional hardware beyond the existing conventional protection, switching, and sensing devices.

2. DISTANCE PROTECTION

Distance protection is based on estimating the line impedance by comparing the fault current passing through the relay against the voltage at the relay point. The feeder length protected by the distance relay is usually divided into three zones or more. Each zone covers a percentage of the line length. For example, zone one usually covers about 85% of the line length from Bus A to Bus B. The second zone covers the entire length of the line connecting Bus A and Bus B plus a portion of the next line length [13, p. 184], and so on for the remaining zones as shown in Figure 2.

The distance relay located at Bus A measures the voltage (V) and current (I) at the fundamental frequency, via voltage and current transformers, respectively. The impedance seen by the relay will be:

$$Z_R = \frac{V_R}{I_R} \tag{1}$$

$$V_R = I_R \cdot \alpha \cdot Z_{line} \tag{2}$$

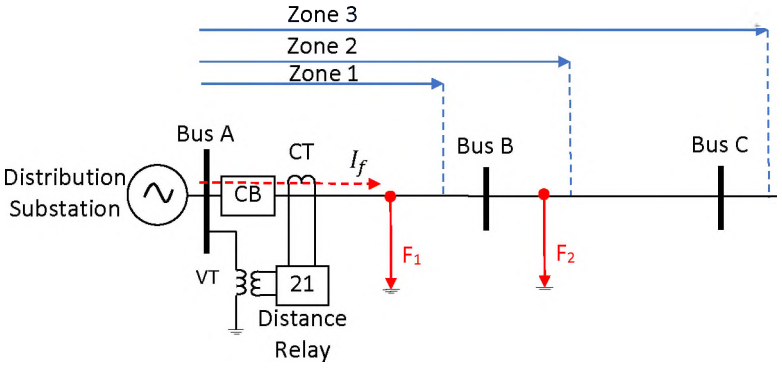

Figure 2. Distance relay protection zones for a radial system.

where V_R and I_R are the voltage and current values measured by the relay, α represents the distance between the relay point and the fault point, and Z_{line} is the impedance of the protected line. The value of the impedance, Z_R, for a fault at F_1 would be

$$Z_R = \alpha \cdot Z_{lineAB} \tag{3}$$

and for a fault at F_2,

$$Z_R = Z_{lineAB} + \alpha \cdot Z_{lineBC} \tag{4}$$

The distance relay operates when the impedance measured by the relay is less than the relay setting value. In other words, the DR will operate if the measured impedance, also known as the apparent impedance, is within its operating characteristic. This characteristic is shown most conveniently in an impedance $R - X$ diagram, where the x-axis represents the resistance R and the y-axis represents the reactance X. There are many different DR characteristics such as mho, impedance, and quadrilateral characteristic. Choosing from these characteristics depends on many factors such as relay design, application, etc. [16]. Figure 3 shows typical DR characteristics on a $R - X$ diagram.

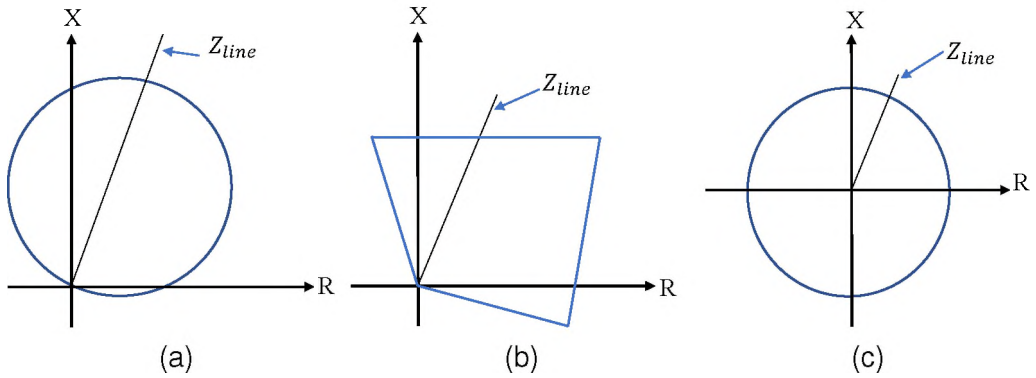

Figure 3. Distance relay characteristics on R-X diagram: (a) mho, (b) quadrilateral, (c) impedance.

3. INFEED EFFECT

The infeed effect causes the impedance seen by the relay to appear to be larger than the actual positive-sequence impedance between the relay and the fault point, causing the relay to underreach. The infeed effects during non-single-line-to-ground (SLG) faults in different configurations are illustrated in Figure 4 and Figure 6 and are described in more detail in following subsections. Each system configuration has a particular infeed effect on the distance relay. For each system, Z_A, Z_B, and Z_C are the line positive-sequence impedances. I_S,I_1,I_2,...,I_n are the currents fed by the sources DG_1, DG_2,..., DG_n. A DR is utilized to protect the feeder in each configuration. The infeed effect on a ground distance relay is described in Subsection 3.3

3.1. CONFIGURATION 1

Figure 4a shows a radial distribution feeder with a generation source at bus B. In the case of a three-phase fault at bus C, the measured voltage by the DR at Bus A would be [13]

$$V_A = I_S Z_A + (I_S + I_1) Z_B \tag{5}$$

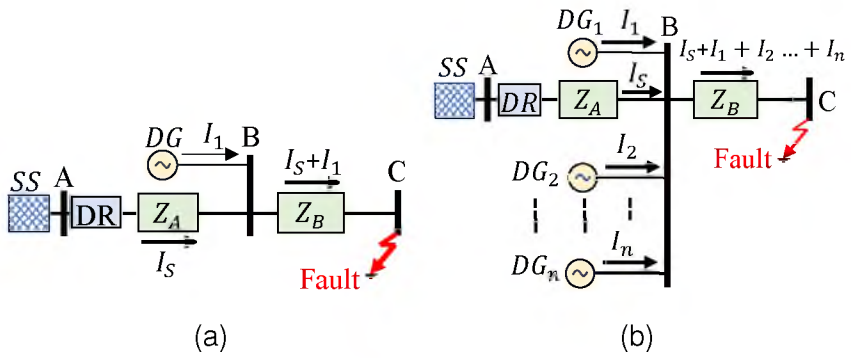

Figure 4. Infeed effect on distance protection: (a) radial distribution feeder with one DG, (b) radial distribution feeder with n DGs connected to the same bus.

The positive-sequence impedance up to the fault location measured by the DR is

$$\begin{aligned} Z_{DR} &= Z_A + (1 + \frac{I_1}{I_S})Z_B \\ &= Z_A + Z_B + K \cdot Z_B \end{aligned} \tag{6}$$

where K is defined as the infeed constant ($K = \frac{I_1}{I_S}$). Based on equation (6), the DR at Bus A measures an impedance larger than the actual impedance between Bus A and the fault point. The additional impedance, KZ_B, impacts the DR operation and the makes DR underreach.

In Figure 4b, more than one DG are connected to the same bus. Their impact on DR measurements would be

$$V_A = I_S Z_A + (I_S + I_1 + I_2 + \ldots + I_n)Z_B \tag{7}$$

The positive-sequence impedance of the line up to the fault point, measured by the DR is

$$\begin{aligned} Z_{DR} &= Z_A + (1 + \frac{I_1 + I_2 + \ldots + I_n}{I_S})Z_B \\ &= Z_A + Z_B + K_n \cdot Z_B \end{aligned} \tag{8}$$

where K_n is the infeed constant ($\frac{I_1+I_2+\ldots+I_n}{I_S} = \frac{\sum_{i=1}^{n} I_i}{I_1}$) and n is the number of DGs connected to Bus B.

The impedance-distance relation in the presence of infeeds is discussed in [13, pp. 186–189]. Figure 5b shows the impedance as a function of the distance for the system in Figure 5a. It is clear that the infeed effect changes the impedance measured by the DR at Bus A. Figure 5b visualizes the impedance measured by the DR in Figure 5a for two different configurations. If there are no DGs in the system, the impedance measured by the DR is equal to the actual impedance of the line, which is proportional to the slope of line segment $A'B'$ in Figure 5a. Integrating a DG into the system changes the impedance measured by the DR, which would be proportional to the slope of the line segment $B'C'$ in Figure 5b. Equations (9) and (10) represent the impedance measured by the DR based on the slope of the line segments in Figure 5b.

$$Z_{DR,AB} = m_{AB} \cdot d = \frac{y_2 - y_1}{x_2 - x_1} \cdot d \tag{9}$$

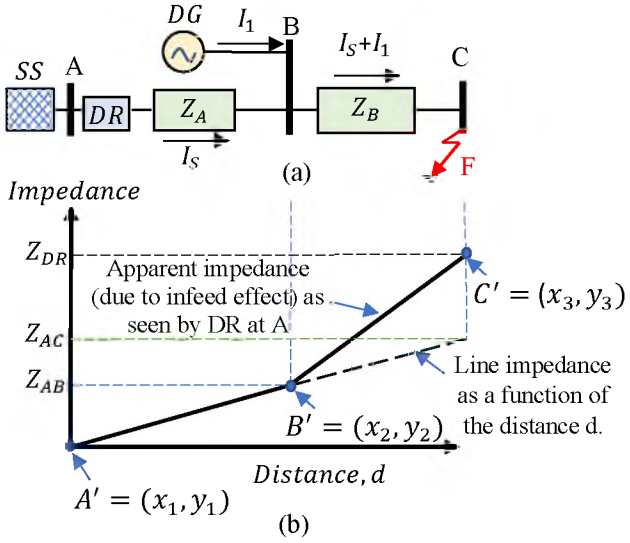

Figure 5. Infeed effect on distance protection: (a) radial distribution feeder with one DG, (b) impedance seen by DR at A.

where $Z_{DR,AB}$ is the measured impedance by the DR if a fault occurs in line AB and m_{AB} is the slope of the line $A'B'$. d is the distance from the relay location up to the fault point. If a fault occurs in line BC, the impedance seen by the DR can be calculated as

$$Z_{DR,BC} = m_{BC} \cdot d = \frac{y_3 - y_2}{x_3 - x_2} \cdot d \tag{10}$$

where $Z_{DR,BC}$ is the measured line impedance seen by the DR at A due to a fault on line BC and m_{BC} is the slope of the line BC.

3.2. CONFIGURATION 2

Figure 6a shows a radial distribution feeder with two generation sources at Buses B and C. In the case of a three line-ground ($3LG$) fault on Bus D, the positive-sequence line impedance up to the fault point measured by the DR at Bus A would be

$$V_A = I_S Z_A + (I_S + I_2) Z_B + (I_S + I_2 + I_3) Z_C \tag{11}$$

$$Z_{DR} = Z_A + (1 + K_1) Z_B + (1 + K_2) Z_C \tag{12}$$

where K_1 is the infeed constant ($K_1 = \frac{I_1}{I_S}$) of line BC and K_2 is the infeed constant ($K_2 = \frac{I_1 + I_2}{I_S}$) of $line\ CD$. In general, if the feeder has n DGs as shown in Figure 6b, the positive-sequence line impedance up to fault position seen by the DR at Bus A would be

$$V_A = I_S Z_A + (I_S + I_2) Z_B + (I_S + I_1 + I_2) Z_C + \ldots + (I_S + I_1 + I_2 + \ldots + I_n) Z_Z \tag{13}$$

$$Z_{DR} = Z_A + (1 + K_1) Z_B + (1 + K_2) Z_C + \ldots + (1 + K_n) Z_Z \tag{14}$$

where K_n is the infeed constant ($\frac{I_1 + I_2 + \ldots + I_n}{I_S} = \frac{\sum_{i=1}^{n} I_i}{I_S}$) for the remote line and n is the number of all DGs on the feeder, and Z_Z is the impedance of the remote line.

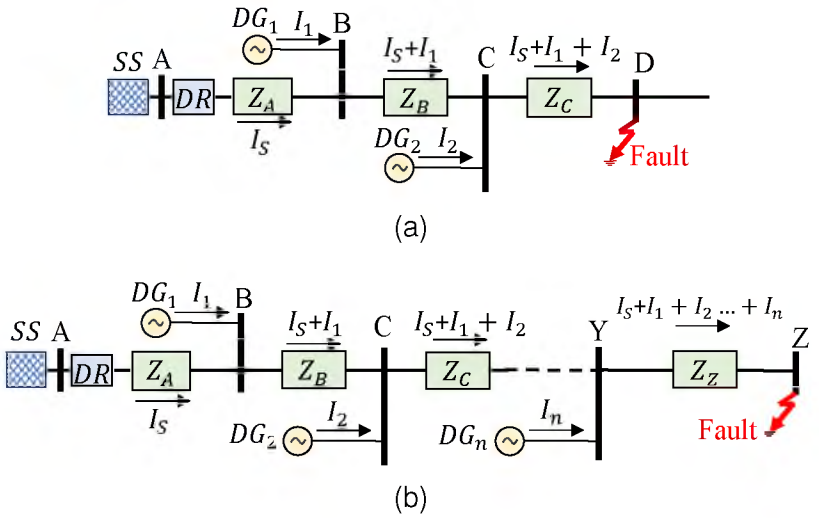

Figure 6. Infeed effect on distance protection: (a) radial distribution feeder with three DGs, (b) radial distribution feeder with n DGs.

3.3. INFEED EFFECT ON GROUND DISTANCE RELAY

A distance relay is designed to measure the positive-sequence impedance of the protected line. However, if a single line-ground (SLG) fault occurs, the measured impedance does not reflect the actual impedance up to the fault location due to the existence of the zero-sequence current. Therefore, the ground distance element (GDE) corrects the measured impedance up to the fault location by applying a compensation factor K_0 [17] which is expressed for most distance relays as [18]

$$K_0 = \frac{Z_0 - Z_1}{Z_1} \tag{15}$$

Hence, the GDE measures the following impedance in case of SLG fault on phase A

$$Z_{GDE_A} = \frac{V_{Ag}}{I_A + K_0 \cdot I_0} \tag{16}$$

where Z_{GDE_A} is the measured impedance by the GDE on phase A in the case of a SLG fault on phase A. V_{Ag} is the phase-A-to-ground voltage ($= \frac{V_A}{\sqrt{3}}$). I_A is the phase A current and Z_0 and Z_1 are the zero and positive sequence impedances of the protected line, respectively. It

should be noted that additional GDEs are required for SLG faults on phases B and C as well. If a SLG fault occurs at point C as shown in Figure 5a, the positive-sequence impedance up to the fault location appears to the GDE as

$$\begin{aligned} Z_{GDE_A} &= \frac{V_{Ag}}{I_A + K_0 \cdot I_0} = Z_A + (1 + \frac{I_1}{I_S})Z_B \\ &= Z_A + Z_B + K \cdot Z_B \end{aligned} \tag{17}$$

Thus, the phase A current has been compensated by K_0 and the GDE measures the positive-sequence impedance to the fault in addition to the additional impedance caused by the infeed effect.

4. PROPOSED METHODOLOGY

The DR does not see the true positive-sequence impedance due to the infeed effect caused by one or more distributed power sources between the main source and the fault location. Many solutions have been proposed to overcome this challenge. However, these solutions are either costly or have other issues related to the reliability of the protection schemes as described earlier. This paper proposes a series of methods that are inexpensive, easy to implement, and do not require communication links to estimate the actual positive-sequence line impedance in the presence of one or more distributed power sources.

4.1. METHOD 1

This method requires the following data: (1) the measured impedance at the relay location; (2) the locations of the DGs; (3) the impedance and the length of the protected line; and (4) fault current calculations (obtained previously from off-line calculations). If the distribution feeder/transmission line has only one power source, as shown in Figure 7a,

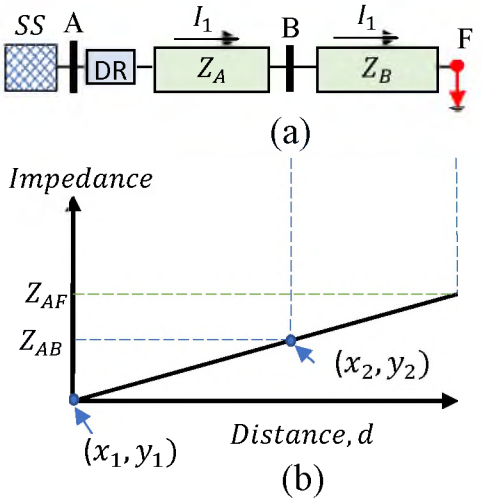

Figure 7. Radial distribution feeder.

the line impedance equation as a function of distance can be written as

$$Z_{DR} = m \cdot d \tag{18}$$

where Z_{DR} is the positive-sequence impedance of the line/feeder corresponding to the distance d. By rearranging (18), the distance d as a function of the impedance can be represented as $d = \frac{Z_{DR}}{m}$.

Figure 8 shows a distribution feeder with a single DG. To develop the proposed method, it is assumed that each line segment has a power source at each bus, except the last bus, which has one DG at its sending end and terminates in a load. For example, line 1-2 in Figure 8 has the substation and DG_1 at its ends, but line 2-3 terminates in a load.

The location/coordinate of the substation is assumed to be $(x_1, y_1) = (0, 0)$ since the DR is located at bus 1. The location/coordinate of DG_1 is (x_2, y_2), where x_2 represents the distance from the DR location to the DG_1 location and y_2 represents the actual positive-sequence line impedance from the DR location to the DG_1 location. The distance x_3 from the DR location to Bus 3 is known, but due to the infeed effect, the impedance y_3 does not

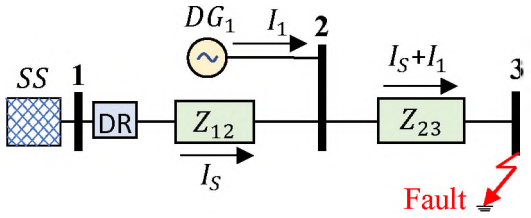

Figure 8. Radial distribution feeder with one DG - method 1.

equal the total positive-sequence to Bus 3. Therefore, the impedance y_3 must be calculated using the following equation:

$$y_3 = Z_{DR} = Z_{12} + Z_{23} + K \cdot Z_{23} \tag{19}$$

where Z_{12} and Z_{23} are the actual positive-sequence line impedances, K is the infeed constant ($K = \frac{I_1}{I_S}$), I_S and I_1 are the fault current contributions from the substation and DG_1 (respectively) for the case of a fault at Bus 3. The fault currents I_S and I_1 for a 3LG fault can be calculated using the following fault calculations:

1. Calculate the Thevenin impedance at the fault location. For the given system:

$$Z_{TH}^{+} = \frac{(Z_S^{+} + Z_{12}^{+})Z_{DG_1}^{+}}{Z_S^{+} + Z_{12}^{+} + Z_{DG_1}^{+}} + Z_{23}^{+} \cdot h \tag{20}$$

   where h is the fractional distance along the length of line 2-3. Note tat $h = 1$ at Bus 3 and $h = 0$ at Bus 2.

2. Calculate the fault current

$$I_{3LG} = \frac{V_f}{Z_{TH}^{+}} \tag{21}$$

   where V_f is the prefault voltage at the fault location, and Z_{TH}^{+} is the Thevenin impedance of the positive-sequence network at the point of the fault from step 1.

3. The fault current contributions from each source can be calculated using the current divider formula:

$$I_S = I_{3LG} \cdot \frac{Z^+_{DG_1}}{Z^+_S + Z^+_{12} + Z^+_{DG_1}} \tag{22}$$

$$I_1 = I_{3LG} \cdot \frac{Z^+_S + Z^+_{12}}{Z^+_S + Z^+_{12} + Z^+_{DG_1}} \tag{23}$$

The actual impedance of the line can be found through leveraging the line equation that represents the impedance measured by the DR versus the distance from the fault for different configurations, i.e., the system with and without DGs. In other words, the impedance measured by DR with and without the infeed effect are compared to find the actual impedance. Equation (24) represents the measured impedance of the line when the infeed effect is considered.

$$Z_{DR} - y_2 = m_2 \cdot (d - x_2) \tag{24}$$

where Z_{DR} is the impedance measured by the DR, x_2 and y_2 represent the coordination of the first point of the faulted line segment, d is the unknown distance from the DR location up to the fault point, m_1 is the slope of the faulted line segment ($m_2 = \frac{y_3 - y_2}{x_3 - x_2}$), and x_3 and y_3 are the coordinates of the remote end of the faulted line segment. Therefore the distance to the fault can be calculated by rewriting (24) as $d = \frac{Z_{DR} - y_2}{m_2} + x_2$. Substituting d into (18), the actual positive-sequence line impedance to the fault point can be obtained:

$$Z_{act} = \frac{m}{m_2}(Z_{DR} - y_2 + m_2 \cdot x_2) \tag{25}$$

Equation (26) is a generalization of (25) that calculates the actual impedance measured by the DR for a system with more than one DG, such as the one shown in Figure 9.

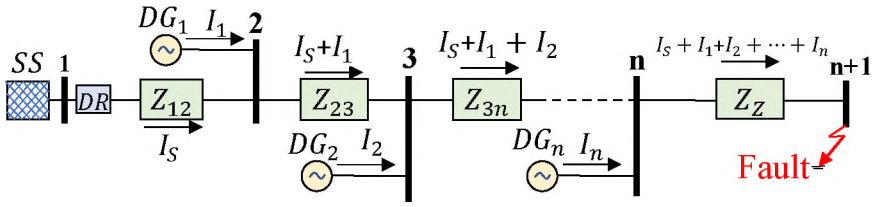

Figure 9. Radial distribution feeder with *nDGs* (proposed method 1).

The actual impedance is given by

$$Z_{act} = \frac{m}{m_i}(Z_{DR} - y_i + m_i \cdot x_i) \tag{26}$$

where m_i is the slope of the faulted line, x_i and y_i are the coordinates of the near end of the faulted line, and i is the Bus number of the faulted segment (i.e., the near end of the faulted segment). The line segmentation data including the location of buses (i.e., x-axis in Figure 5b), impedance of the lines (i.e., y-axis in Figure 5b), and fault currents should be calculated offline and stored in the DR. To calculate the actual impedance of the line, the fault location in the system must be known. To this end, we propose an approach that iteratively compares the impedance of the line segments stored in DR with the impedance measured by the DR. Figure 10a illustrates the different steps of this approach. Finding the faulty section provides the impedance and distance from the DR of the underlying line, which helps to calculate the actual impedance measured by the DR according to (26). A simplified schematic diagram of Method 1 is shown in Figure 10b. The control logic in Figure 10b contains the required equations to calculate the infeed constant, K, the line slope for each line segment, and the proposed logic steps to determine the faulted segment of the line as explained in Figure 10a.

As an example, consider the simple distribution feeder shown in Figure 11. Assume that the length of line AB is 2.5 km and Z_A = 2.5 Ω and the length of line BC is 4.5 km and Z_B = 4.5 Ω. For a 3LG bolted fault at point C, I_S and I_1 are 0.176/80.02° kA and 1.576/−9.88° kA, respectively. Therefore, the impedance measured by the DR at Bus A

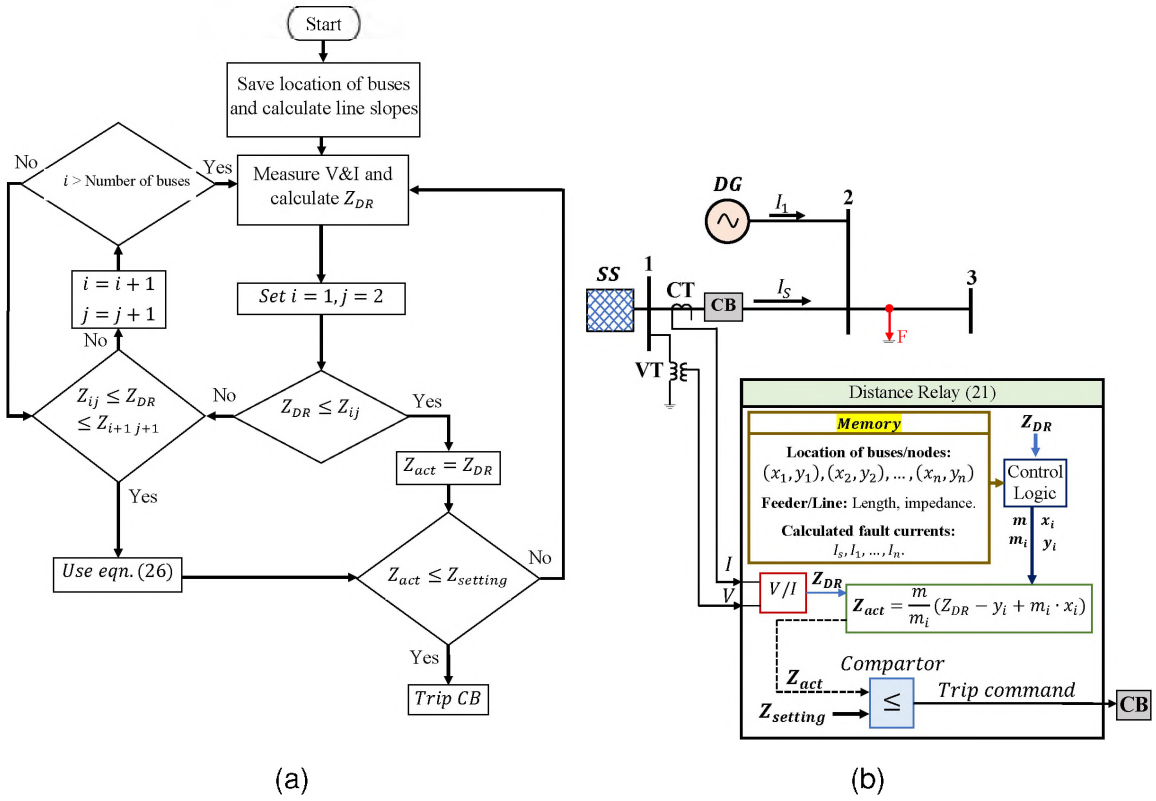

Figure 10. (a) Flowchart of the proposed Method 1, (b) Simplified schematic diagram of Method 1.

can be calculated using (8).

$$\begin{aligned} Z_{DR} &= Z_A + Z_B + K \cdot Z_B \\ &= 2.5 + 4.5 + (8.93\underline{/-89.9°}) \cdot 4.5 \\ &= 40.8\underline{/-80.02°}\ \Omega \end{aligned}$$

where K is $\frac{I_1}{I_S} = 8.93\underline{/-89.9°}$. Note that the DR at A measures an impedance of 40.8 $\underline{/-80.02°}$ Ω for a fault at C. This is larger than the actual impedance from A to C, which is only 7 Ω. Based on the proposed approach, the feeder's actual impedance to the fault

location can be calculated:

$$m = \frac{2.5 - 0}{2.5 - 0} = 1$$
$$m_1 = \frac{40.8\angle -80.02° - 2.5}{7 - 2.5} = 8.988\angle -83.51°$$

$$\begin{aligned} Z_{act} &= \frac{m}{m_1}(Z_{DR} - y_1 + m_1 x_1) \\ &= \frac{1}{m_1}(40.8\angle -80.02° - 2.5 + m_1 \cdot 2.5) = 7\,\Omega \end{aligned}$$

which is equal to the actual impedance of the feeder to the faulty point. It is notable that the infeed effect has no impact on the calculation.

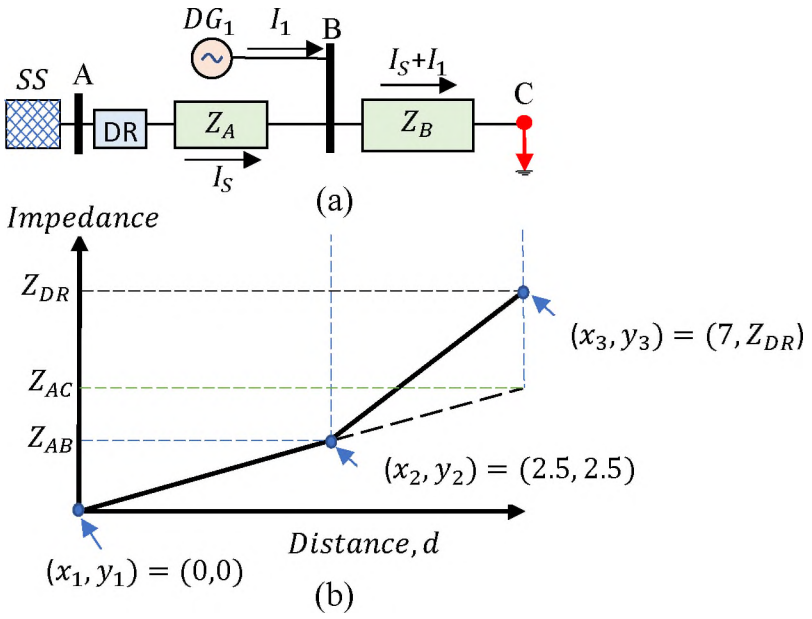

Figure 11. Radial distribution feeder.

4.2. METHOD 2

Method 2 is based on creating two impedance-distance (ID) curves similar to the plot in Figure 5b. The first ID curve (ID curve-1) represents the relation between the impedance and the distance of the feeder with DGs, whereas the second ID curve (ID curve-2) represents the impedance-distance relation of the same feeder with one power source (i.e., the main source at the beginning of the feeder/line). The impedance-distance curves should be created offline and stored in the DR. Data storage and offline calculations (even the online calculations if necessary) are not difficult for modern relays that contain large memories and advanced processors. To find the actual line impedance, Z_{act}, the measured impedance, Z_{meas}, should be compared with the ID curve-1 to find the corresponding value of the distance. Then the distance value will be compared with the ID curve-2 to get Z_{act} as shown in Figure 12. In the case of a 3LG fault, the following steps illustrate the plotting of the line segment $B'C'$ in Figure 5b:

1. Calculate the Thevenin impedance at the fault location. For the given system,

$$Z_{TH}^{+} = \frac{(Z_S^{+} + Z_A^{+})Z_{DG}^{+}}{Z_S^{+} + Z_A^{+} + Z_{DG}^{+}} + Z_B^{+} \cdot d \tag{27}$$

   where d is the fractional distance along the length of feeder/line. Note that $d = 1$ at Bus C and $d = 0$ at Bus B. Z_S^{+} & Z_{DG}^{+} are the positive-sequence impedances of the substation and DG, respectively. Z_A^{+} and Z_B^{+} are the positive-sequence impedances of line AB and line BC, respectively.

2. Calculate the fault current as

$$I_{3LG} = \frac{V_f}{Z_{TH}^{+}} \tag{28}$$

where V_f is the prefault voltage at fault location, and Z_{TH}^{+} is the Thevenin impedance of the positive-sequence network at the point of the fault from step 1.

3. The fault current contributions from each power source can be calculated using the current divider formula as follows

$$I_S = I_{3LG} \cdot \frac{Z_{DG}^{+}}{Z_S^{+} + Z_A^{+} + Z_{DG}^{+}} \tag{29}$$

$$I_1 = I_{3LG} \cdot \frac{Z_S^{+} + Z_A^{+}}{Z_S^{+} + Z_A^{+} + Z_{DG}^{+}} \tag{30}$$

4. Calculate the infeed constant, $K = \frac{I_1}{I_S}$.

5. Calculate the impedance value corresponding to the value of d using the following equation

$$Z_{DR} = Z_A^{+} + (1 + K)Z_B^{+} \cdot d \tag{31}$$

6. Change the value of d in descending order (in small steps) from 1 to 0 and repeat steps 1-5 for each d value.

7. Plot the impedance vs. distance curve.

Figure 12a and Figure 12b present a flowchart and the simplified schematic diagram of the proposed Method 2.

4.3. METHOD 3

This method has the advantage of not requiring any offline calculations and is only based on the local measurements. It also requires the location and impedance of the infeed source to calculate the location of the fault. This data, in addition to the impedance and

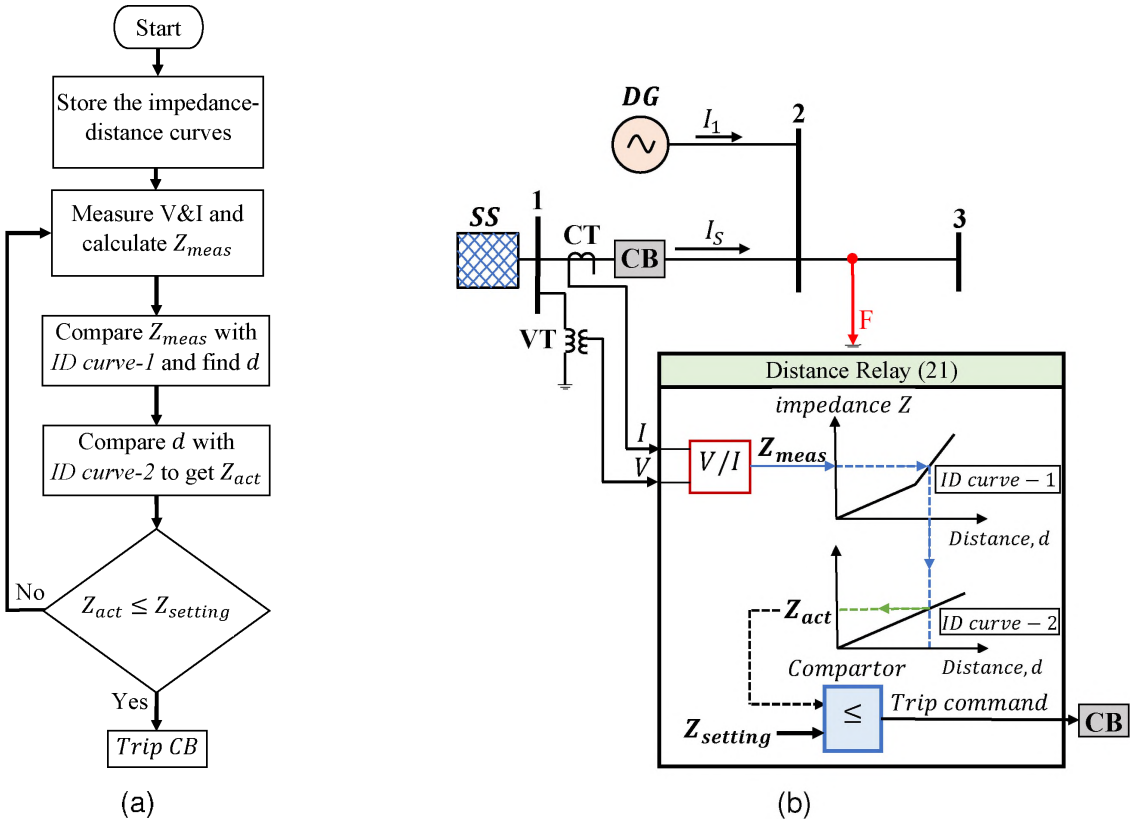

Figure 12. (a) Flowchart of the proposed Method 2, (b) Simplified schematic diagram of Method 2.

length of the feeder/line, which are usually known and stored in the DR as "inputs", can be used to locate the fault without any need for measurements from the remote source. Figure 13a will be used to illustrate the principle of this method.

The system in Figure 13a consists of two sources at Buses 1 and 2. The main source, SA, is connected to Bus 1 and the second source, SB,is connected to Bus 2. SB can be either a strong source or a weak source. A strong source may be a feeder from another substation or a large synchronous generator, whereas a weak source may be an Inverter-Based Resource (IBRs), such as solar or wind power [19]. To clarify how the proposed method works, we explain it for the "strong source" case under two fault types: 3LG fault and SLG faults.

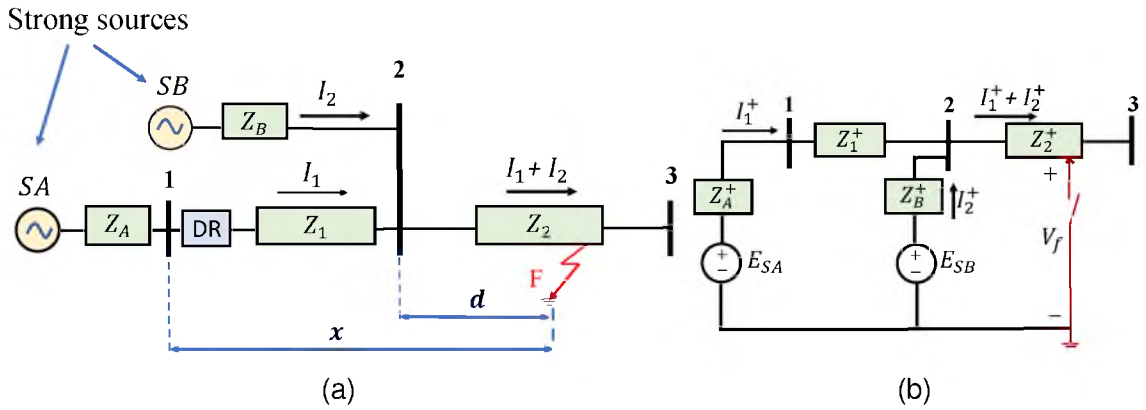

Figure 13. (a) Radial distribution feeder-Method 3, (b) The positive-sequence equivalent circuit.

4.3.1. 3LG Fault. For a 3LG fault, as shown in Figure 13a, fault currents from SA and SB contribute to the total fault current. Each fault current is a positive-sequence current because the fault is a symmetrical fault. The per-phase equivalent circuit of the system is shown in Figure 13b. The impedance measured by the DR can be calculated as follows

$$Z_{DR} = Z_1 + Z_2 \cdot d \cdot (1 + \frac{I_2}{I_1}) \tag{32}$$

and the 3LG fault current at fault location can be calculated as

$$I_{3LG} = \frac{V_f}{Z_{TH}^+} \tag{33}$$

where V_f is the prefault voltage at the fault location. Z_{TH}^+ is the positive-sequence Thevenin impedance which can be calculated as

$$Z_{TH}^+ = \frac{(Z_A^+ + Z_1^+)Z_B^+}{Z_A^+ + Z_1^+ + Z_2^+} + Z_2^+ \cdot d \tag{34}$$

$$= \alpha^+ + Z_2^+ \cdot d \tag{35}$$

Substituting (35) into (33), yields

$$I_{3LG} = \frac{V_f}{\alpha^+ + Z_2^+ \cdot d} \tag{36}$$

Using the current-divider formula, the fault current contribution from SB can be calculated as

$$I_2 = I_{3LG} \cdot \frac{Z_A^+ + Z_1^+}{Z_A^+ + Z_1^+ + Z_B^+} \tag{37}$$

$$= I_{3LG} \cdot \gamma^+ \tag{38}$$

Substituting (33) into (38), yields

$$I_2 = \frac{V_f}{\alpha^+ + Z_2^+ \cdot d} \cdot \gamma^+ \tag{39}$$

Similarly, substituting (39) into (32), the impedance Z_{DR} is obtained:

$$Z_{DR} = Z_1^+ + Z_2^+ \cdot d \cdot \left(1 + \frac{\frac{V_f}{\alpha^+ + Z_2^+ \cdot d} \cdot \gamma^+}{I_1}\right) \tag{40}$$

Solving (40) for d, yields two possible solutions:

$$d_1, d_2 = -\frac{I_1 {Z_1}^+ - I_1 Z_{DR} + I_1 \alpha^+ + V_f \gamma^+ \mp \beta}{2 \cdot I_1 \cdot {Z_2}^+} \tag{41}$$

where

$$\beta = [{I_1}^2 \cdot ((Z_1^+)^2 + Z_{DR}(-2Z_1^+ + Z_{DR} + 2\alpha^+) + (\alpha^+)^2) + I_1 \cdot (-2Z_1^+\alpha + V_f\gamma^+ \cdot (2Z_1^+ - 2Z_{DR} + 2\alpha)) + {V_f}^2(\gamma^+)^2]^{\frac{1}{2}} \tag{42}$$

Equation (41) has two solutions with different signs in which only the positive one (d_2 in this case) would be valid. Equation (41) calculates the distance from the SB location to the fault location. Thus, the actual positive-sequence impedance from the DR location to the fault location can be calculated as

$$Z_{DR}^{act} = {Z_1}^+ + {Z_2}^+ \cdot d_2 \tag{43}$$

Therefore, the per-unit distance, x, from the DR location to the fault location is

$$x = \frac{Z_{DR}^{act}}{Z_1{}^{+} + Z_2{}^{+}} \tag{44}$$

4.3.2. SLG Fault. The single line to ground (SLG) fault is the most common fault that occurs in electrical networks in general and in overhead lines in particular. The SLG fault, along with line-to-line (LL) and line-to-line-to-ground (LLG) faults, are called unbalanced faults. Symmetrical components must be used for solving unbalanced faults. The positive-sequence Thevenin impedance viewed from the fault location can be computed by (35). The negative-sequence Thevenin impedance is usually equal to the positive-sequence Thevenin impedance. Thus, it can be written as

$$Z_{TH}^{-} = \frac{(Z_A^{-} + Z_1^{-})Z_B^{-}}{Z_A^{-} + Z_1^{-} + Z_2^{-}} + Z_2^{-} \cdot d \tag{45}$$

$$= \alpha^{-} + Z_2^{-} \cdot d \tag{46}$$

The zero-sequence Thevenin impedance is

$$Z_{TH}^{0} = \frac{(Z_A^{0} + Z_1^{0})Z_B^{0}}{Z_A^{0} + Z_1^{0} + Z_2^{0}} + Z_2^{0} \cdot d \tag{47}$$

$$= \alpha^{0} + Z_2^{0} \cdot d \tag{48}$$

The symmetrical components of the fault current are

$$I_f{}^{0} = I_f{}^{+} = I_f{}^{-} = \frac{V_f}{Z_{TH}{}^{0} + Z_{TH}{}^{+} + Z_{TH}{}^{-}} \tag{49}$$

The fault current is

$$I_f = 3I_f{}^{0} = \frac{3V_f}{Z_{TH}{}^{0} + Z_{TH}{}^{+} + Z_{TH}{}^{-}} \tag{50}$$

Applying current-divider formula, the symmetrical components of the fault current contribution from SB can be expressed as

$$I_2^0 = \frac{Z_A^0 + Z_1^0}{Z_A^0 + Z_1^0 + Z_B^0} \cdot I_f^0 \tag{51}$$

$$= \gamma^0 \cdot I_f^0 \tag{52}$$

$$I_2^+ = \frac{Z_A^+ + Z_1^+}{Z_A^+ + Z_1^+ + Z_B^+} \cdot I_f^+ \tag{53}$$

$$= \gamma^+ \cdot I_f^+ \tag{54}$$

$$I_2^- = \frac{Z_A^- + Z_1^-}{Z_A^- + Z_1^- + Z_B^-} \cdot I_f^- \tag{55}$$

$$= \gamma^- \cdot I_f^- \tag{56}$$

Therefore, the fault current in phase a is

$$I_2 = {I_2}^0 + {I_2}^+ + {I_2}^- = 3{I_2}^+ \tag{57}$$

Substituting for I_2 in the infeed constant, $K = \frac{I_2}{I_1}$, yields

$$K = \frac{3{I_2}^+}{I_1} \tag{58}$$

$$= \frac{3\gamma^+ I_f^+}{I_1} \tag{59}$$

$$= \frac{\frac{3 \cdot V_f \cdot \gamma^+}{\alpha^0 + Z_2^0 \cdot d + \alpha^+ + Z_2^+ \cdot d + \alpha^- + Z_2^- \cdot d}}{I_1} \tag{60}$$

Z_{DR} can be expressed based on d by substituting (60) in (40),

$$Z_{DR} = Z_1^+ + Z_2^+ \cdot d \cdot \left(1 + \frac{\frac{3 \cdot V_f \cdot \gamma^+}{\alpha^0 + Z_2^0 \cdot d + \alpha^+ + Z_2^+ \cdot d + \alpha^- + Z_2^- \cdot d}}{I_1} \right) \tag{61}$$

Solving for d yields

$$d = -\frac{I_1 Z_2^- Z_1^+ \mp \sqrt{I_1^2[a + 2Z_2^-(b - c - d + e + f + g) + h - i - j + k + L + m)] + r + s} + v}{2I_1 Z_2^+ (Z_2^0 + Z_2^+ + Z_2^-)} \quad (62)$$

where

$$a = (Z_2^-)^2 \cdot ((Z_2^+)^2 - 2Z_1^+ Z_{DR} + Z_{DR}^2) \quad (63)$$

$$b = (Z_1^+)^2 \cdot (Z_2^+ + Z_2^0) \quad (64)$$

$$c = Z_1^+ Z_2^+ \cdot (2Z_{DR} + \alpha^0 + \alpha^+ + \alpha^-) \quad (65)$$

$$d = 2Z_1^+ Z_2^0 Z_{DR} \quad (66)$$

$$e = Z_2^+ Z_{DR}^2 \quad (67)$$

$$f = Z_2^+ Z_{DR} \alpha^- \quad (68)$$

$$g = Z_{DR}(Z_2^+(\alpha^0 + \alpha^+) + Z_2^0 Z_{DR}) \quad (69)$$

$$h = (Z_1^+)^2 \cdot ((Z_2^+)^2 + 2Z_2^+ Z_2^0 + (Z_2^0)^2) \quad (70)$$

$$i = 2Z_1^+ (Z_2^+)^2 \cdot (Z_{DR} + \alpha^0 + \alpha^+ + \alpha^-) \quad (71)$$

$$j = 2Z_1^+ Z_2^+ Z_2^0 \cdot (2Z_{DR} + \alpha^0 + \alpha^+ + \alpha^-) \quad (72)$$

$$k = Z_{DR} \cdot (-2Z_1^+ (Z_2^0)^2) + (Z_2^+)^2 \cdot (Z_{DR} + 2(\alpha^0 + \alpha^+ + \alpha^-)) \quad (73)$$

$$L = (Z_2^+)^2 \cdot ((\alpha^-)^2 + 2\alpha^-\alpha^+ + 2\alpha^-\alpha^0 + (\alpha^+)^2 + 2\alpha^+\alpha^0 + (\alpha^0)^2) \quad (74)$$

$$m = 2Z_2^+ Z_2^0 \cdot (Z_{DR}^2 + Z_{DR}(\alpha^0 + \alpha^+ + \alpha^-) + (Z_2^0)^2 Z_{DR}^2 \quad (75)$$

$$r = 6I_1 V_f \gamma^+ \cdot (Z_2^- Z_2^+ (Z_1^+ - ZDR) + (Z_2^+)^2 (Z_1^+ - Z_{DR} + \alpha^0 + \alpha^+ + \alpha^-) \quad (76)$$

$$s = Z_2^+ Z_2^0 (Z_1^+ - Z_{DR})) + 9V_f^2 (Z_2^+)^2 (\gamma^+)^2 \quad (77)$$

$$v = I_1[Z_1^+(Z_2^+ + Z_2^0) - Z_{DR}(Z_2^0 + Z_2^+ + Z_2^-) + Z_2^+(\alpha^0 + \alpha^+ + \alpha^-)] + 3V_f Z_2^+ \gamma^+ \quad (78)$$

Equation (62) has two solutions with different signs in which only the positive one, d_2, would be valid. Moreover, it is important to note that Z_{DR} is the corrected measured impedance as explained in Section 3.3. Equation (62) calculates the distance from the SB location to

the fault point. Thus, the actual positive-sequence impedance from the DR location to the fault location can be calculated as

$$Z_{DR}^{act} = Z_1{}^{+} + Z_2{}^{+} \cdot d_2 \tag{79}$$

Therefore, the per-unit distance, x, from the DR location up to the fault location is

$$x = \frac{Z_{DR}^{act}}{Z_1{}^{+} + Z_2{}^{+}} \tag{80}$$

Figure 14a and Figure 14b present a flowchart and the simplified schematic diagram of the proposed method 3.

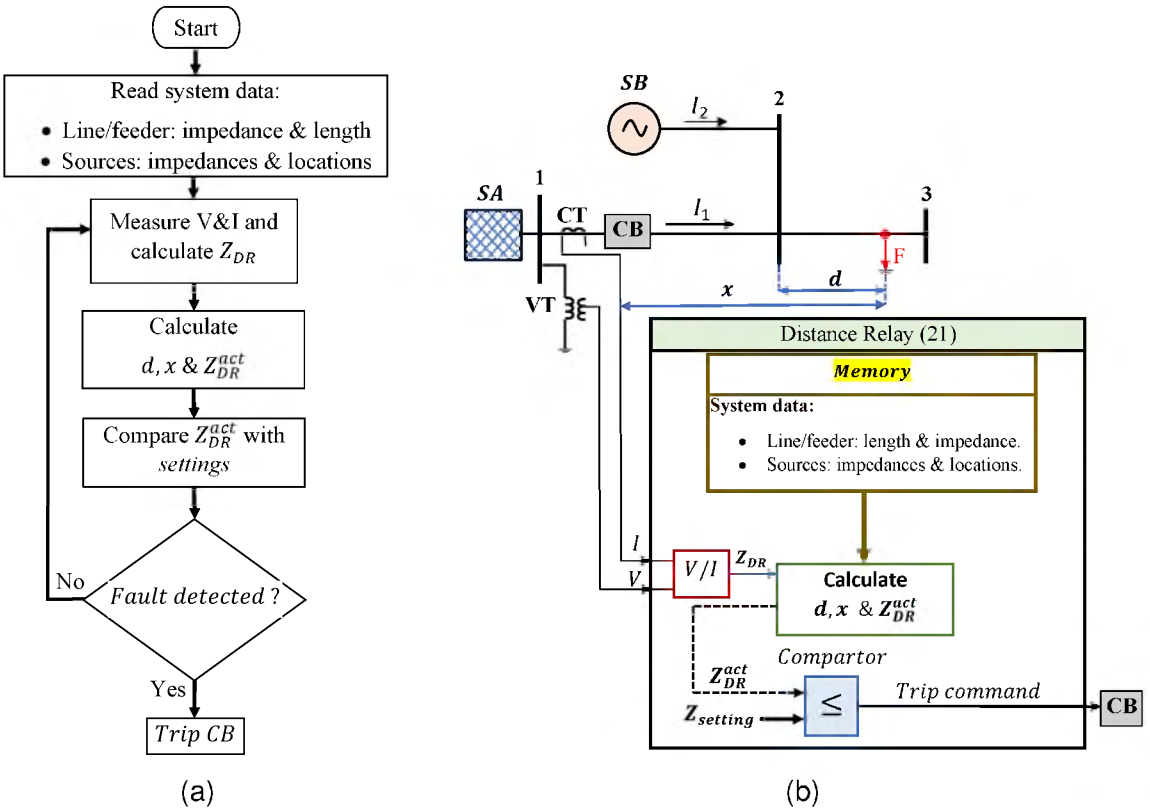

Figure 14. (a) Flowchart of the proposed Method 3, (b) Simplified schematic diagram of Method 3.

5. SIMULATION RESULTS

A comparison of the three proposed methods including discussion is given in this section.

5.1. TEST SYSTEM DESCRIPTION

Figure 15 shows the radial 12.47 kV, 60 Hz distribution feeder used in the simulation analysis. The distribution feeder has two segments, each segment is 10 km long and has the following positive and zero sequence impedances, $z_1 = (0.9507 + j \cdot 1.948) \cdot 10^{-4}$ Ω/m, and $z_0 = (0.2403 + j \cdot 0.6019) \cdot 10^{-3}$ Ω/m. The substation is fed by an interconnected transmission grid through a step-down distribution transformer. The upstream transmission grid and the distribution transformer are represented by a Thevenin equivalent voltage source with positive and zero sequence impedances of $Z_1^{eq} = 0.298\underline{/89.9°}$ Ω and $Z_0^{eq} = 0.233\underline{/89.9°}$ Ω respectively. A 12.47 kV power source is also connected to the feeder at Node B which is 10 km away from the substation or DR location. The power source could be any type of strong power source, such as a synchronous generator, etc. In this simulation, we intentionally consider a larger power source at node *B*, i.e. 12.47 kV with 553.8 MVA short-circuit power, in order to have a power source with a higher infeed current contribution during the fault. The feeder is protected by the DR with mho characteristics phase and ground elements at the head of the line (i.e., at Node A). The studied distribution system is modeled using PSCAD™/EMTDC™ [20].

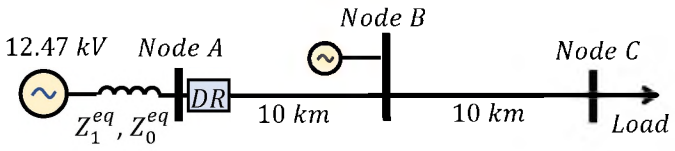

$$z_1 = (0.9507 + \mathrm{j} \cdot 1.948) \cdot 10^{-4}\ \Omega/\mathrm{m}$$
$$z_0 = (0.2403 + \mathrm{j} \cdot 0.6019) \cdot 10^{-3}\ \Omega/\mathrm{m}$$

Figure 15. One-line diagram of a simplified distribution feeder.

5.2. DISTANCE RELAY SETTINGS

Two zones are set to cover the entire feeder (from node A to node C). Zone 1 and zone 2 are set to cover 80% and 130% of the positive-sequence feeder impedance, respectively. The positive-sequence line impedance is $4.3352\angle 64°$ Ω. The first and second zone reach are therefore $0.8 \times 4.3352\angle 64° = 3.47\angle 64°$ Ω and $1.3 \times 4.3352\angle 64° = 5.64$ at 64° Ω, respectively. Zones 1 and 2 are shown in Figure 16 with green and blue mho characteristic in the complex impedance plane, respectively. For the faults located at 0-80% from the DR, the DR operates immediately. However in practice, fault isolation requires a few cycles (i.e., 6-18 cycles at 60 Hz or 0.1-0.3 s) depending on the relay decision-making process and the speed of the CB [16]. The operating time for zone 2, typically, is in the range of 0.4-0.5 s [21]. Therefore, the first zone time delay is set to be 0.1 s, whereas the operating time for zone 2 is 0.45 s. The zero-sequence compensation factor K_0 is calculated and stored in the ground distance element (GDE) in order to allow the reach settings to be specified in terms of positive-sequence impedance [6]. K_0 can be calculated using (15)

$$K_0 = \frac{Z_0 - Z_1}{Z_1} = 0.6647\angle 6.38° \tag{15}$$

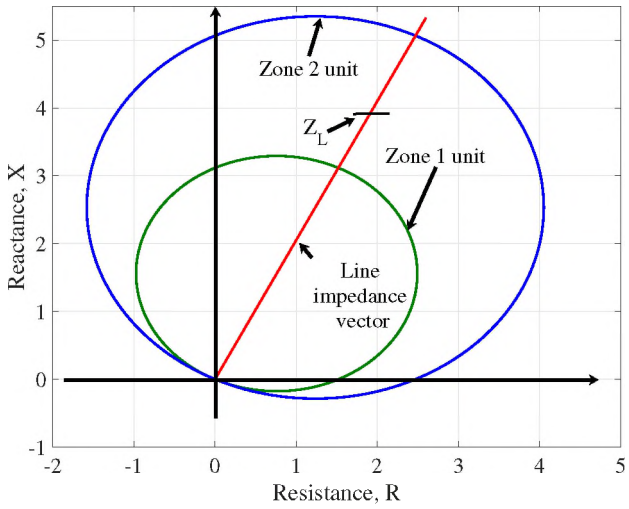

Figure 16. Operating characteristic of distance protection located at Node A.

Converting the impedance from the primary side to the secondary side of the CT and PT transformers does not have any impact on the proposed method and thus we directly utilize the impedance on the primary side in this paper.

5.3. STUDY CASES

In order to carefully analyze the proposed methods, many fault scenarios with different fault locations and fault types were investigated. The case studies were selected to test the efficiency and accuracy of the proposed methods in measuring the feeder's actual positive-sequence impedance in the event of faults at different distances along the distribution feeder inside and outside of the protection zones of the distance protection. In all of the case studies, there are two power sources: the distribution substation at the head of the distribution feeder (i.e., at Node A) and a power source connected to node B as shown in Figure 15. The study cases are for bolted 3LG and SLG faults at a distance of 40%, 70%, 100%, and 140% of the distribution feeder length. Figure 17 shows the fault locations and the DR scheme used in the case studies.

5.3.1. Case I: Fault at a Distance of 40% of the Feeder's Length. The objective of this case is to establish the effectiveness of the proposed methods in the event of a fault between the substation and the power source at node B (i.e., within the boundaries

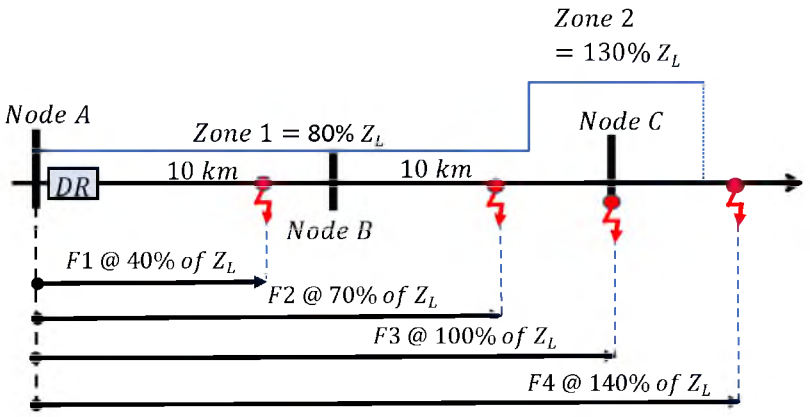

Figure 17. DR scheme using two protection zones and fault locations.

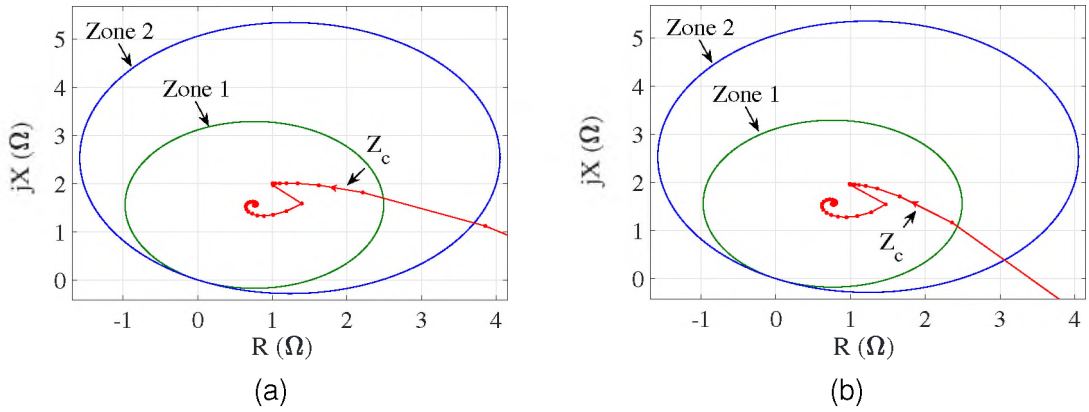

Figure 18. Impedance trajectory for (a) 3LG and (b) SLG fault at 40% of the feeder's length.

of Zone 1). Figure 18a shows the plot of the impedance seen by the DR for a 3LG fault located at F1 (see Figure 17 for fault locations). Since the infeed effect does not affect the reading of the DR, the measured impedance is correct and is the actual positive-sequence impedance between the DR location and fault location. Therefore, the zone 1 element provides tripping with a time of 0.1 s, which is the correct function of the DR. Similarly, Figure 18b demonstrates the impedance trajectory in the case of the SLG fault. Z_c denotes the conventionally measured impedance.

5.3.2. Case II: Fault at a Distance of 70% of the Feeder's Length. The objective of this case is to establish both the effectiveness and accuracy of the proposed methods on the DR's measurements. Figure 19a and Figure 19b show the DR performance in the case of 3LG and SLG faults. We observed that the impedance measured by the conventional DR, Z_c, is out of the operating zones of the DR, although the fault is within the operating characteristic of zone 1. However, the impedance measured by the proposed methods, Z_{m1} (Method 1), Z_{m2} (Method 2), and Z_{m3} (Method 3), are all located within the zone 1 area. Numerically, the measured impedance Z_c to the fault at the DR location for a 3LG fault is 2.39 pu, rather than the actual positive-sequence impedance of 0.7 pu. On the other hand, the impedance measured by the proposed methods Z_{m1}, Z_{m2} and Z_{m2} are all equal to 0.7 pu. The measured impedance Z_c is 3.69 pu for a SLG fault at F2 while the measured impedance

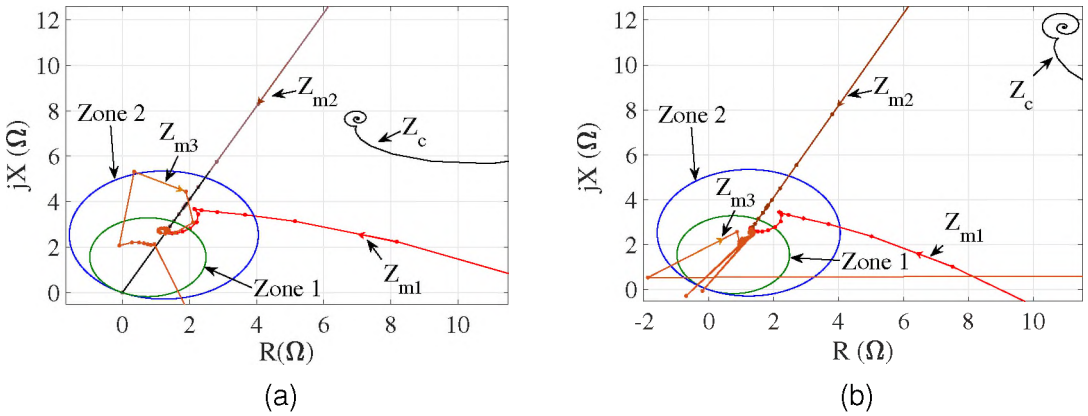

Figure 19. Impedance trajectories of the proposed and conventional methods for (a) 3LG fault and (b) SLG fault at 70% of the feeder's length.

by the proposed methods Z_{m1}, Z_{m2} and Z_{m2} are 0.7 pu, 0.7 pu, and 0.68 pu which are the same, or close to, the actual positive-sequence impedance from the DR location to the fault point F2.

5.3.3. Case III: Fault at a Distance of 100% of the Feeder's Length. In this case, the fault location is outside of zone 1 but within the boundaries of zone 2. As shown in Figure 20a and Figure 20b, Z_{m1}, Z_{m2}, and Z_{m3} trajectories move into zone 2. However, the Z_c trajectory is out of the operating zones of the DR. Therefore, Z_{m1}, Z_{m2}, and Z_{m3} reflect the correct impedance trajectory. Thus, the DR trip will be delayed by the time setting of

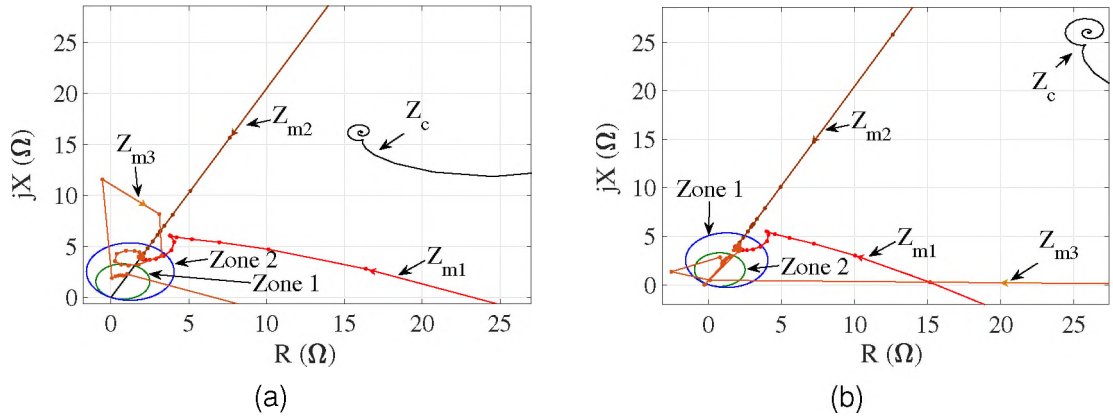

Figure 20. Impedance trajectories of the proposed and conventional methods for (a) 3LG fault and (b) SLG fault at 100% of the feeder's length.

zone 2 which is set at 0.45 s. The measured Z_c for a 3LG fault at F3 is 5.26 pu whereas the Z_{m1}, Z_{m2}, and Z_{m3} are all equal to 1 pu for the same fault. Similarly, the measured Z_c is 8.49 pu for SLG fault whereas Z_{m1}, Z_{m2}, and Z_{m3} are 1.0 pu, 1.0 pu, and 1.01 pu which are the same, or close to, the actual positive-sequence impedance from the DR location to the fault point F3.

5.3.4. Case IV: Fault at a Distance of 140% of the Feeder's Length. The impedance trajectories seen by the DR in the case of 3LG and SLG faults at F4 are plotted in Figure 21a & Figure 21b, respectively. In this case the fault location is outside the operating characteristic of zone 2. Figure 21a and Figure 21b show that the Z_{m1}, Z_{m2}, Z_{m3} are outside zone 2 as is expected. Thus, the DR does not trip, reflecting a correct decision of the DR. The measured Z_c for a 3LG fault at F4 is 9.09 pu whereas the Z_{m1}, Z_{m2}, and Z_{m3} are all equal to 1.4 pu for the same fault. Similarly, the measured Z_c is 14.84 pu for SLG fault while Z_{m1}, Z_{m2}, and Z_{m3} are 1.4 pu, 1.4 pu, and 1.48 pu which are the same, or close to, the actual positive-sequence impedance from the DR location to the fault point F4.

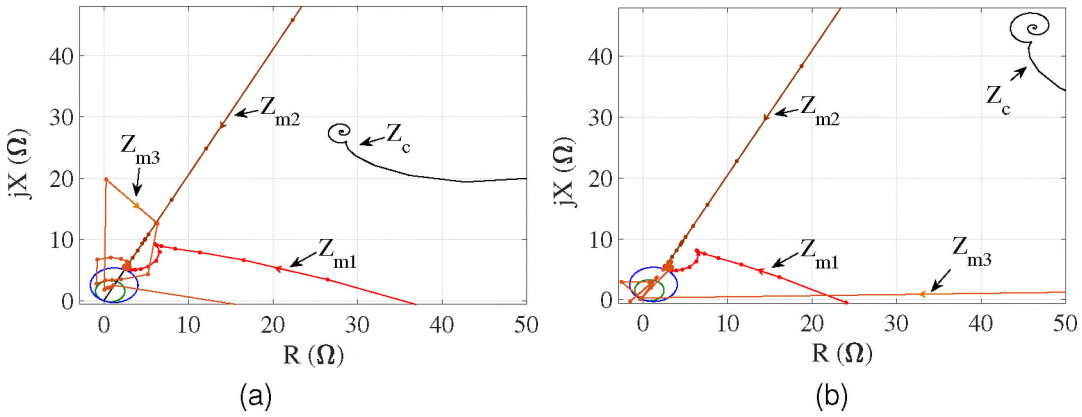

Figure 21. Impedance trajectories of the proposed and conventional methods for (a) 3LG fault and (b) SLG fault at 140% of the feeder's length.

Table 1 summarizes the results of the different case studies. The impedance values are in pu based on the magnitude of the positive-sequence impedance of the distribution feeder ($|Z_{base}| = 4.3352\,\Omega$). Z_{act} in the 4th column is the actual positive-sequence

impedance in pu of the distribution feeder. Z_{m1}, Z_{m2}, and Z_{m3}, in the 6th-8th columns, are the measured impedances by the proposed methods 1, 2, and 3, respectively. Similar observations have been made for both line-line and line-line-ground faults.

Table 1. Distance relay performance under varying system conditions.

Fault type	Fault location	Zone protection	Z_{act} (pu)	Measured impedance, pu			
				Z_c	Z_{m1}	Z_{m2}	Z_{m3}
3LG	F1	1	0.4	0.4	0.4	0.4	0.4
	F2	1	0.7	2.39	0.7	0.7	0.7
	F3	2	1.0	5.26	1.0	1.0	1.0
	F4	Out of zones	1.4	9.09	1.4	1.4	1.4
SLG	F1	1	0.4	0.4	0.4	0.4	0.4
	F2	1	0.7	3.69	0.7	0.7	0.68
	F3	2	1.0	8.49	1.0	1.0	1.01
	F4	Out of zones	1.4	14.84	1.4	1.4	1.48

5.4. COMPARISON OF METHODS

Each of the proposed methods has its own technique for determining the location of the fault. Different features of the proposed methods including the required data and calculations, cost, and results accuracy are compared to clarify the differences between them.

1. Required data and calculations: All three methods require local measurements and the system's data in order to determine the fault location in the presence of an infeed current. In addition to the system data and local measurements, the first and second methods require the results of offline calculations in order to determine the fault location. The first method requires calculating the offline fault current values as part of the data to be stored in the DR. Similarly, the second method requires calculating offline fault currents to create ID curves. The third method has an advantage over the first two methods in that it does not require any offline calculations and its functionality entirely depends on local measurements.

2. Cost: The functionality of three methods proposed in this paper do not require the addition of any measuring or communication devices. In other words, the proposed methods do not incur any additional hardware cost to the current system.

3. Accuracy of the results: One of the most important indicators of the success for any method is its accuracy. To this end, all the proposed methods have been tested using PSCAD™/EMTDC™ software. The results proved the capability of the proposed methods in locating the faults with high accuracy in the presence of an infeed effect. Method 3 is the least accurate due to its dependence purely on on-line measurements with no off-line calculations, but the drop in accuracy may be counter-balanced by its other advantages.

Table 2 presents a summary comparison of the proposed methods.

Table 2. Proposed methods comparison.

Proposed Methods	**Required data and calculations**	**Cost**	**Accuracy of the results**
Method 1	• Local measurements • System data • Offline calculations	Very low	Very high
Method 2	• Local measurements • System data • Offline calculations	Very low	Very high
Method 3	• Local measurements • System data	Very low	High

6. CONCLUSIONS

In this paper, the impact of the infeed effect caused by one or more power sources between the main source and the fault location on distance relay functionality is studied. Previously published works on protection schemes for transmission lines/distribution feeders using distance relays have provided either costly or low reliability solutions. Increasing

amounts of renewable generation in distribution system increases the infeed current which challenges the current protection scheme. To address this issue, three new methods that estimate the distance to the fault in the presence of the infeed effect have been proposed in this paper. These methods are applicable for distance relays, whether in radial distribution feeders or transmission lines. The accuracy of the proposed methods are examined using different case studies. The obtained results indicates the potential superiority of the proposed methods over similar proposed methods.

BIBLIOGRAPHY

[1] Gonen, T. *Electric Power Distribution Engineering*, Third ed., Boca Raton: CRC Press, 2014, p. 769.

[2] X. Tong and J. Liu, "Fault Processing Based on Local Intelligence," in *Fault Location and Service Restoration for Electrical Distribution Systems*, Singapore, John Wiley & Sons, 2016, p. 32.

[3] El-Khattam, W.; Sidhu, T.S. "Restoration of Directional Overcurrent Relay Coordination in Distributed Generation Systems Utilizing Fault Current Limiter," in *IEEE Transactions on Power Delivery*, vol. 23, no. 2, pp. 576-585, April 2008, doi: 10.1109/TPWRD.2008.915778.

[4] Singh, M.; Vishnuvardhan, T.; Srivani, S.G. "Adaptive protection coordination scheme for power networks under penetration of distributed energy resources," *IET generation, transmission & distribution*, 2016, 10, pp. 3919–3929.

[5] Singh, M.K.; Reddy, P.N. "A fast adaptive protection scheme for distributed generation connected networks with necessary relay coordination," *2013 Students Conference on Engineering and Systems (SCES)*, 2013, pp.1–5. doi:10.1109/SCES.2013.6547562.

[6] Sinclair, A.; Finney, D.; Martin, D.; Sharma, P. "Distance Protection in Distribution Systems: How It Assists With Integrating Distributed Resources," in *IEEE Transactions on Industry Applications*, vol. 50, no. 3, pp. 2186-2196, 2014, doi: 10.1109/TIA.2013.2288426.

[7] Chang, J.; Gara, L.; Fong, P.; Kyosey, Y. "Application of a multifunctional distance protective IED in a 15KV distribution network," *2013 66th Annual Conference for Protective Relay Engineers*, 2013, pp. 150–171. doi:10.1109/CPRE.2013.6822034.

[8] Enayati, A.; Ortmeyer, T.H. "A novel approach to provide relay coordination in distribution power systems with multiple reclosers," *2015 North American Power Symposium (NAPS)*, 2015, pp. 1–6. doi:10.1109/NAPS.2015.7335121.

[9] Tsimtsios, A. M.; Nikolaidis, V.C. "Setting Zero-Sequence Compensation Factor in Distance Relays Protecting Distribution Systems," in *IEEE Transactions on Power Delivery*, vol. 33, no. 3, pp. 1236-1246, June 2018, doi: 10.1109/TPWRD.2017.2762465.

[10] Ziegler, G. *Numerical distance protection: principles and applications*; John Wiley & Sons, 2011.

[11] Verzosa, Q. "Understanding the various methods of residual compensation setting the resistive reach of polygon characteristics and ways of modeling and testing the relay," *Proc. 32nd Annu. Western Protective Relay Conf.*, 2005, pp. 1–33.

[12] Blackburn, J.L.; Domin, T.J. *Protective relaying: principles and applications*; CRC press, 2015; pp. 600–602.

[13] Gers, J.M.; Holmes, E.J. *Protection of electricity distribution networks*; Vol. 47, IET, 2011.

[14] Biswas, S.; Centeno, V. "A communication based infeed correction method for distance protection in distribution systems," *2017 North American Power Symposium (NAPS)*, 2017, pp. 1–5. doi:10.1109/NAPS.2017.8107226

[15] Anderson, P.M. *Power System Protection*; Wiley-IEEE Press, 1999; p. 379.

[16] Kezunovic, M.; Ren, J.; Lotfifard, S. *Design, modeling and evaluation of protective relays for power systems*; Springer, 2016.

[17] Horowitz, S.H.; Phadke, A.G. *Power system relaying*; John Wiley & Sons, 2014; p. 111.

[18] Nikolaidis, V.C.; Tsimtsios, A.M.; Safigianni, A.S. "Investigating Particularities of Infeed and Fault Resistance Effect on Distance Relays Protecting Radial Distribution Feeders With DG," *IEEE Access*, 2018, 6, 11301–11312. doi:10.1109/ACCESS.2018.280404.

[19] Jones, K.W.; Pourbeik, P.; Kobet, G.; et al. Impact of inverter based generation on bulk power system dynamics and short-circuit performance. Technical Report PES-TR68, *IEEE Power & Energy Society*, 2018.

[20] M. H. International, "PSCAD version 5.0," Manitoba Hydro International Ltd. (MHI), [Online], Available: https://www.pscad.com/. [Accessed 01 06 2021].

[21] Ibrahim, M.A. *Disturbance Analysis for Power Systems*, 1st ed.; Wiley: Hoboken, N.J, 2011; p. 223.

II. A NEW APPROACH TO PROTECTION COORDINATION FOR DISTRIBUTION SYSTEMS WITH DISTRIBUTED GENERATION

Fahd A. Hariri, and Mariesa L. Crow
Department of Electrical & and Computer Engineering
Missouri University of Science and Technology
Rolla, Missouri 65409–0050
Email: fahrz9@mst.edu

ABSTRACT

In power distribution systems, the protection systems are designed to isolate faults in a coordinated manner among protective devices to ensure the continuity of the service with a minimum impact on customers. The integration of distributed generation (DG) can enhance power quality and reliability and decrease power losses, environmental pollution, and the cost of network expansions. However, the higher penetration of DGs increases the short-circuit current levels of distribution systems which in turn can change the direction of the fault currents. Thus, the current designed coordination scheme between protection devices may no longer be sufficient to ensure correct operation. This paper proposes a new approach to limit the fault current in distribution systems by controlling single-phase inverters that connect DGs to distribution systems. First, we develop a new approach to control single inverter-based distributed generation (IBDG) and then model the distribution systems with IBDG. We finally elaborate the proposed method by conducting a single-line-to-ground fault on the proposed model in the PSCAD™/EMTDC™ environment. This paper concludes with a discussion of how this approach can be extended to different fault types and system configurations.

1. INTRODUCTION

In conventional power networks, the generated energy is transmitted from generating stations via transmission lines to distribution substations. Distribution substations distribute power to consumers through overhead lines or underground cables. However, this traditional power transmission method has some drawbacks, such as high energy production costs, environmental concerns due to using fossil fuels, and a high amount of active power losses during the transmission and distribution processes. Small DGs that are connected to distribution systems (DSs), as shown in Figure 1, have small sizes (about 100 kW to 10 MW) [1].

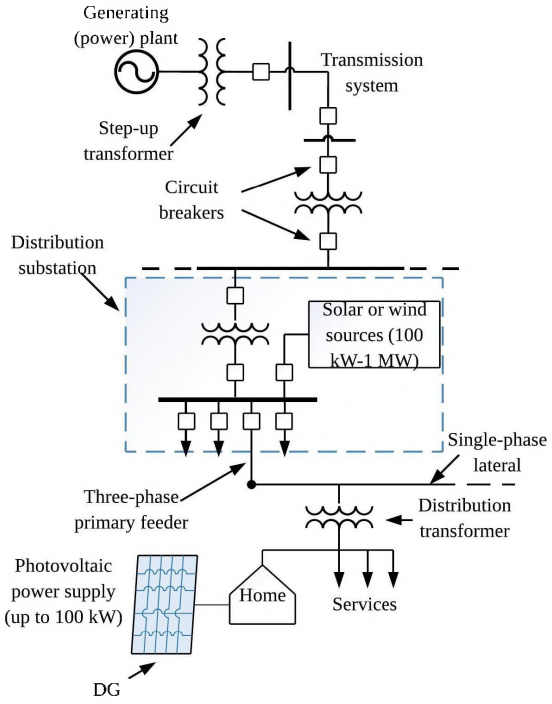

Figure 1. Integration of DGs into the utility system.

Wind turbines, photovoltaics (PV), microturbines, internal combustion engines, batteries, diesel generators, and gas turbines are examples of DG technologies. DG technologies can be divided into IBDG and non-IBDG. The former is known as IBDG due to an inverter interface necessary to synchronize the DG with the primary grid. IBDG includes

PV, wind power, and energy storage. Non-IBDGs include electric rotating machinery such as synchronous generators and induction generators. Integration of DGs into the electric power networks has changed many transmission and distribution concepts. For example, connecting DGs near loads gives essential advantages such as reducing active power losses and meeting increased load demands without expanding in building new generating stations.

Despite many advantages that DGs have brought to the distribution system, they can complicate existing DS protection due to their impact on fault currents. For example, the protection coordination of the system in Figure 2a is designed based on the unidirectional power flow from the substation to loads. If a temporary fault occurs at F, the recloser tries to eliminate the fault by de-energizing the main feeder many times. If the fault is not eliminated, the fuse isolates the fault. In this system, the fault current passing through the recloser and fuse has the same magnitude.

By contrast, if a DG is connected somewhere between the recloser and the fuse, as shown in Figure 2b, the magnitude of fault current contribution passing through the recloser is less than the previous case in Figure 2a, and therefore both the fuse and the recloser see different fault currents. The fuse sees a higher fault current than the recloser. Therefore, coordination between them is no longer effective. As a result, the fuse will burn out before the recloser operates, which will cut off power to all consumers connected to that tapped lateral.

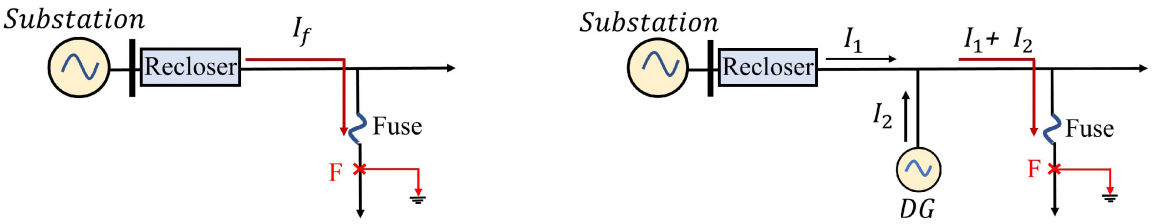

Figure 2. (a) Radial distribution line with no DGs, and (b) Radial distribution line with a DG.

Each DG technology has its own short-circuit characteristics. The peck value of short-circuit current for non-inverter-based distributed generation is very high [2–4]. On the other hand, IBDGs have limited contribution to fault current due to their control strategy and the thermal capability of their switching elements, e.g., Insulated-Gate Bipolar Transistors (IGBTs) [2]. The development of future electrical systems will need to accommodate the impact of all these generation types.

Various protection strategies have been proposed to maintain and improve the protection of DSs along with fully exploiting DGs. These approaches can be classified as either remedial methods or preventive methods [5]. The remedial method depends on reconfiguring the existing protection system (e.g., changing the settings of the overcurrent devices to maintain the existing protection scheme [6]). One drawback of remedial methods is tedious job of resetting overcurrent relays, which is even more evident in large systems [7]. Limiting the short-circuit current of the DG is the main objective of the preventive method. Many approaches have been proposed to control and limit fault currents in the distribution system embedded with DGs using fault current limiters (FCLs). Changing the impedance of FCLs and their locations when the DS and/or DG are reconfigured is proposed in [8–10]. The cost of the FCL is directly related to the value of its impedance under the fault conditions. Thus, the larger impedance value of the FCL, the higher the cost [9]. Some important factors are discussed in [11–13], such as the numbers and sizes of FCLs as well as their optimal locations in the radial distribution system. The approach proposed in [14] maintains the protection system coordination in the presence of DGs without modifying the protection scheme using the instantaneous disconnection of all DGs during the fault. The major disadvantage of this method is that all DGs are disconnected each time a fault occurs. This works well for permanent faults but is overly cautious for temporary faults. The primary motivation behind the proposed protection strategy presented herein is to minimize implementation costs while maintaining the original structure of the DS. Therefore, the proposed strategy does not change the existing conventional protection schemes.

2. PROPOSED APPROACH

In rural areas, distribution systems primarily consist of overhead lines. Almost 80 % to 95% of the faults in distribution systems are temporary faults [15]. These faults are called transient faults and usually happen if a phase conductor momentarily touches another phase or ground. Causes of such faults can be lightning, trees, birds, or other animals. Therefore, many utilities started employing a fuse-saving strategy to ensure supply reliability by avoiding what is known as sustained outages caused by temporary faults.

2.1. FUSE SAVING PROTECTION SCHEMES

The strategy to save the fuse on the lateral feeder from a temporary fault is accomplished by de-energizing the main feeder with an upstream interrupting device, such as a recloser before the downstream fuse can blow. The function of the recloser in the fuse-saving scheme is to trip on fast mode before the operation of the downstream fuse and then reclose to allow power restoration in a short time. If the fault persists, the delayed mode of the recloser will activate. This delayed action pushes the lateral fuse to isolate the fault [16]. This scheme depends mainly on the time-current characteristic (TCC) curves which coordinate the operating sequence between the recloser and fuse. The fuse saving scheme used in most of the distribution system protection schemes is designed on the fact that the DS has a unidirectional flow of power from the substation to the loads downstream. However, as discussed previously, the penetration of DGs changes the DS from being a passive unidirectional system to an active bidirectional system. Therefore, the current situation of the existing protection systems faces new challenges that require some adjustments to address this new functionality. As noted, some of the impacts of the integration of DGs may include changes in the direction of the power flow, the change of fault current level, or false tripping of feeders (i.e., sympathetic tripping) [17], [18]. Subsequently, DGs may

affect the coordination between the recloser and the downstream fuses caused by additional short-circuit current contributions from the DGs during the fault. Consequently, the fuse could blow before the recloser, leading to higher operational costs and unnecessary customer service loss.

This paper proposes a new approach to limit fault currents by controlling IBDGs, particularly single-phase inverter-based PV resources. It will be shown that this proposed approach is capable of maintaining coordination between reclosers and fuses on radial distribution feeders in the presence of DGs by limiting the fault current contribution during temporary faults. Since the majority of faults in radial distribution systems are single-line-to-ground (SLG) faults [19], [20], this paper focuses on SLG faults. The proposed method herein is an improvement over other proposed methods in that it allows a fuse-saving approach regardless of the size of DG, whereas other proposed approaches limit the size of the deployed DG to limit the fault current [21], [22]. Therefore, this approach is low-cost and easy to apply.

As discussed in section I, the presence of DGs complicates the existing protection of DSs because of their impact on fault currents both in level and direction. The research aims to introduce a new way to reduce the negative impact on protection coordination due to the presence of IBDGs on the distribution systems by reducing their fault current contribution under temporary SLG fault.

2.2. INVERTER-BASED DG

The single-phase inverter has many different topologies. For example, a voltage-source inverter (VSI) has a constant input voltage, and its output voltage does not change with load conditions. Similarly, the current-source inverter (CSI) output current remains constant, and the output current is kept constant irrespective of load conditions. Inverters can be classified as full-bridge inverters or half-bridge inverters based on how many switch legs

each type has. The full-bridge inverter, as shown in Figure 2b, also known as an H-bridge, consists of two legs with two IGBTs. Inverters typically use the pulse-width-modulation (PWM) technique to produce an ac output voltage [23].

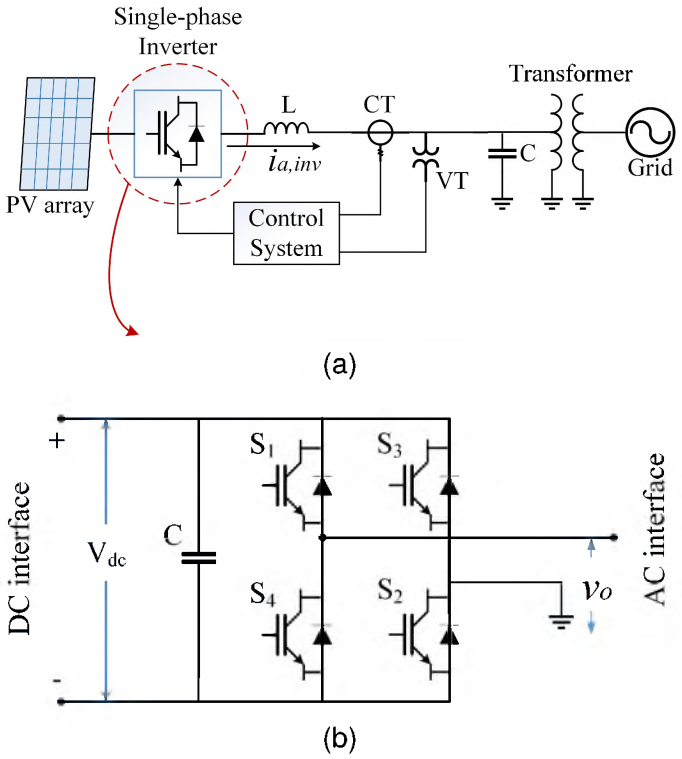

Figure 3. (a) Grid-connected system; (b) Single-phase full-bridge converter.

2.3. PROPOSED IBDG FAULT CURRENT LIMITING SCHEME

The proposed approach is based on the principle that the reactance of inductors varies with frequency as:

$$Z_L = \omega L = 2\pi f L \tag{1}$$

where f is the frequency in hertz, and L is the inductance in Henries. Based on (1), the reactance changes linearly with frequency; therefore, higher frequencies result in higher reactance. The output current of the inverter has a fundamental frequency equal to the reference signal. Therefore, the output frequency is controllable by changing the reference

signal. The reference signal of the PWM can be sinusoidal or any other waveshapes. Moreover, it must be generated within the control circuit of the inverter or from outside reference [24]. This important feature of the PWM is the backbone of the proposed method of this paper.

Figure 4 shows the flowchart of the proposed approach. The flowchart starts with measuring the IBDG output current. If the fault occurs somewhere in DS, the control circuit activates the high-frequency mode which is explained in the next paragraph. As noted above, the inductor acts as an open circuit at very high frequencies, thereby limiting the fault current contribution from the IBDG. When the fault is cleared, the frequency of the IBDG switches back to 60 Hz to keep the IBDGs connected to the system. Thus, the proposed approach can successfully handle temporary faults. For a permanent fault, the IBDGs will be disconnected, similar to other methods.

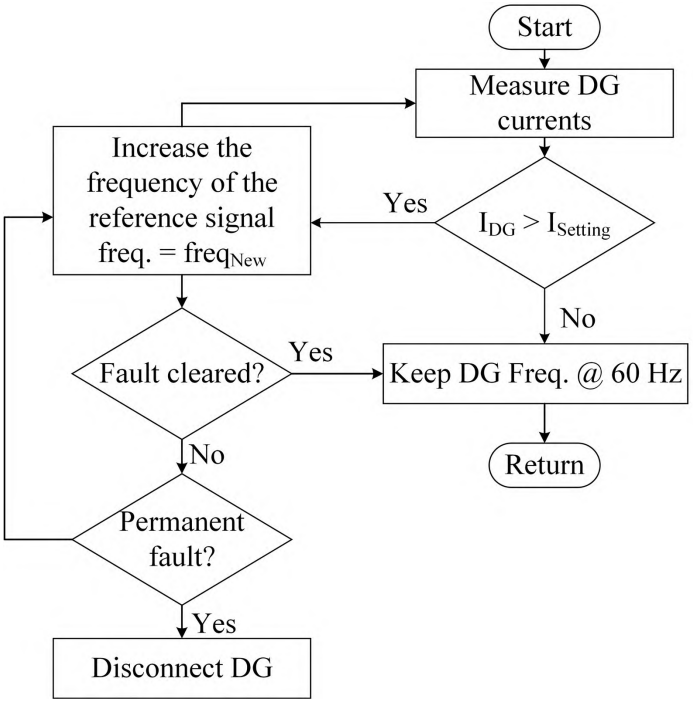

Figure 4. Flowchart of the proposed method.

Figure 5 shows the schematic configuration of the proposed control system for the grid-connected inverter with the current control mode. The scheme consists of two modes: Normal Mode (NM) and Emergency Mode (EM). A mode selector is connected to these two modes to alternate between them. When the fault occurs, the fault detection algorithm inside the IBDG senses the fault and sends an activation signal to the mode selector to activate the EM. Once the fault is over, the fault detection algorithm sends a signal to the mode selector to reactivate the NM.

In the NM, the gate pulses to the inverter IGBTs are generated by comparing the reference and carrier waveforms. Thus, the inverter output frequency is controllable by the reference signal frequency, which is the grid frequency in NM (i.e., nominally 60 Hz). On the other hand, the required frequency of the inverter's output current in the EM can be

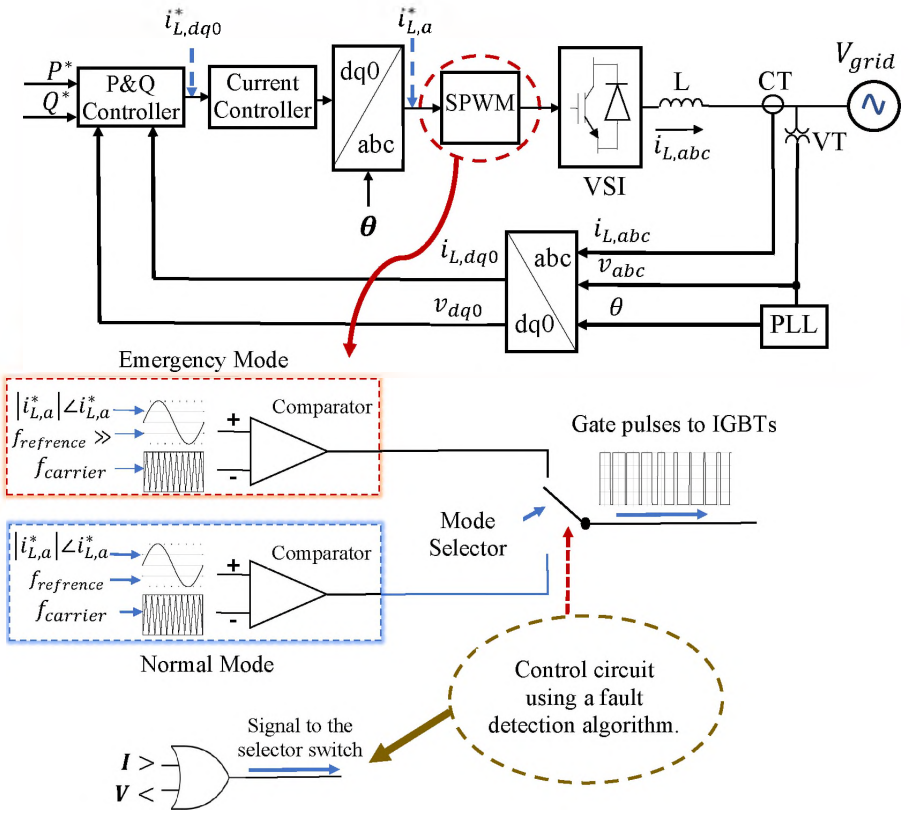

Figure 5. Schematic configuration of the proposed control system of the grid-connected inverter with current control mode.

estimated or determined based on the specifications of the inverter used and the required reduction in fault current contribution of the IBDG. For instance, the frequency of the reference signal can be raised to a high value (e.g., 6 kHz) if the inverter used contains switches capable of withstanding this high frequency. Therefore, the inverter's output current frequency increases as the frequency of the reference signal increases.

Let us assume we have a simple DS system for ease of understanding, as shown in Figure 6a. The IBDG interfaces with the system by the inductor, L. This inductor filters out the current of the IBDG. During a fault condition, IBDG fault current contribution is limited to 1-3 of its maximum current, $I_{max.}$. Using the proposed approach, the frequency of the reference signal will be switched to high frequency. Therefore, depending on (1), the reactance of the inductor, X_L, will be increased until it acts as an open circuit, as shown in Figure 6b. Thus, the fault current contribution of IBDG decreases to almost zero. Mathematically, IBDG current contribution can be expressed as

$$I_{IBDG} = \begin{cases} 1to3 \cdot I_{max} & \text{for normal mode,} \\ \approx 0 & \text{for emergency mode.} \end{cases} \tag{2a}$$

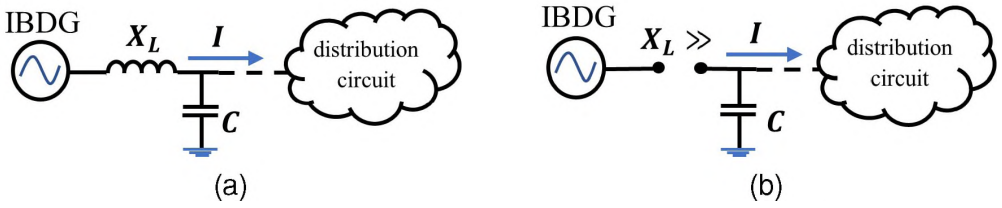

Figure 6. Simple DS.

3. PROPOSED METHOD VALIDATION

This section demonstrates the behavior of the conventional protection scheme for distribution feeder in the presence of DG and compares that with the proposed method. Four different cases including (1) base system, (2) base system with IBDG and conventional

protection, (3) base system with IBDG and the proposed protection method, and (4) base system with IBDG and a Resistive Superconducting Fault Current Limiter (SFCL), demonstrate the effectiveness of the proposed method. Finally, a comparison is presented between these cases and their behaviors during the operation of protective devices. This study is restricted to single-phase faults, and it can be easily extended to consider other types of faults. Simulation studies in this paper have been conducted using the PSCAD™/EMTDC™ software [25].

3.1. CASE 1: BASE SYSTEM

As shown in Figure 7, the system includes a feeder connected to the distribution substation through a step-down transformer. A recloser protects the main feeder, and a fuse protects the lateral. The protection scheme used in this feeder is a fuse-saving scheme with two fast and two delayed sequences. Table 1 shows the parameter values used for the simulations. The recloser and fuse data used in these tests are taken from ASPEN OneLiner™ software's library [26]. Figure 8 shows the screenshot from ASPEN OneLiner™ software of the TCC curves (excluding the annotations) for the recloser and fuse. Case 1 has been divided into a temporary and permanent fault, depending on the SLG fault duration.

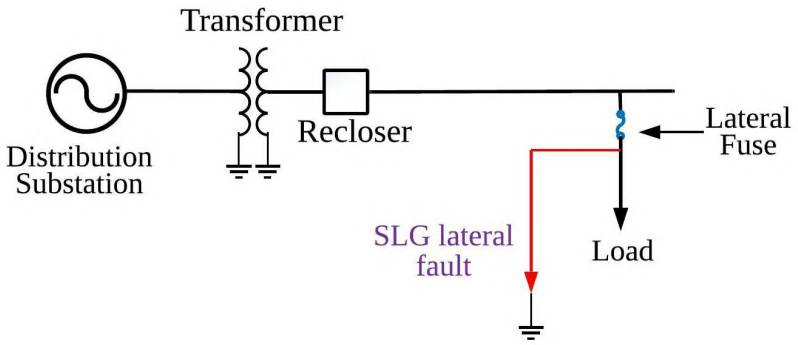

Figure 7. Single-phase test system diagram for case 1.

Table 1. Parameter values of the test system

Parameters	**Value**
Source: Line–line Input voltage (RMS)	4.6 kV
Source impedance type	$R = 0.1\ \Omega$
Power frequency	60 Hz
Fault Nature	LG fault

First, a temporary SLG fault is applied at $t = 0.7\ s$ on the single-phase lateral. Only phase A will experience a short-circuit condition, while the other will not be affected. The fault current seen by the recloser on phase A exceeds the minimum setting for a ground pickup current. In this case, the fault current is 3.421 kA, and the pickup current setting is 290 A; therefore, the first fast operation will be performed at $t = 0.723\ s$ depends on the fast TCC curve, as shown in Figure 8 (i.e., it trips after 0.023 s or two cycles). The fast recloser action is operated before the fuse could blow. As a result, the fuse would be saved from melting. The recloser stays open for 0.2 s during its first reclose interval to let the fault be self-cleared. We assumed that the fault lasts for 0.5 s, so at $t = 0.956\ s$, the recloser will perform the second fast operation. The second recloser interval lasts for 0.5 seconds. During the second reclose interval, the temporary fault would be cleared due to the recloser action. The recloser closes back at time $t = 1.467\ s$ to pass the load current of 69 A. Figure 9a shows the output of the simulation for the temporary fault on phase A.

Second, a permanent SLG fault is applied at $t = 0.7\ s$ on the single-phase lateral. Since the fault is permanent, the two-fast operation of the recloser at $t = 0.723\ s$ and $t = 0.956\ s$, will not isolate the fault. The recloser switches to its delay-time TCC curve to allow the fuse to blow and isolate that lateral at $t = 1.563\ s$ depends on the fast TCC curve, as shown in Figure 8 (i.e., it needs 0.0963 s or 5.78 cycles to melt and isolate the fault). As a result, at $t = 1.563\ s$, the fuse current goes to zero, which means complete isolation of the fault. Figure 9b shows the output of the simulation for the permanent fault on phase

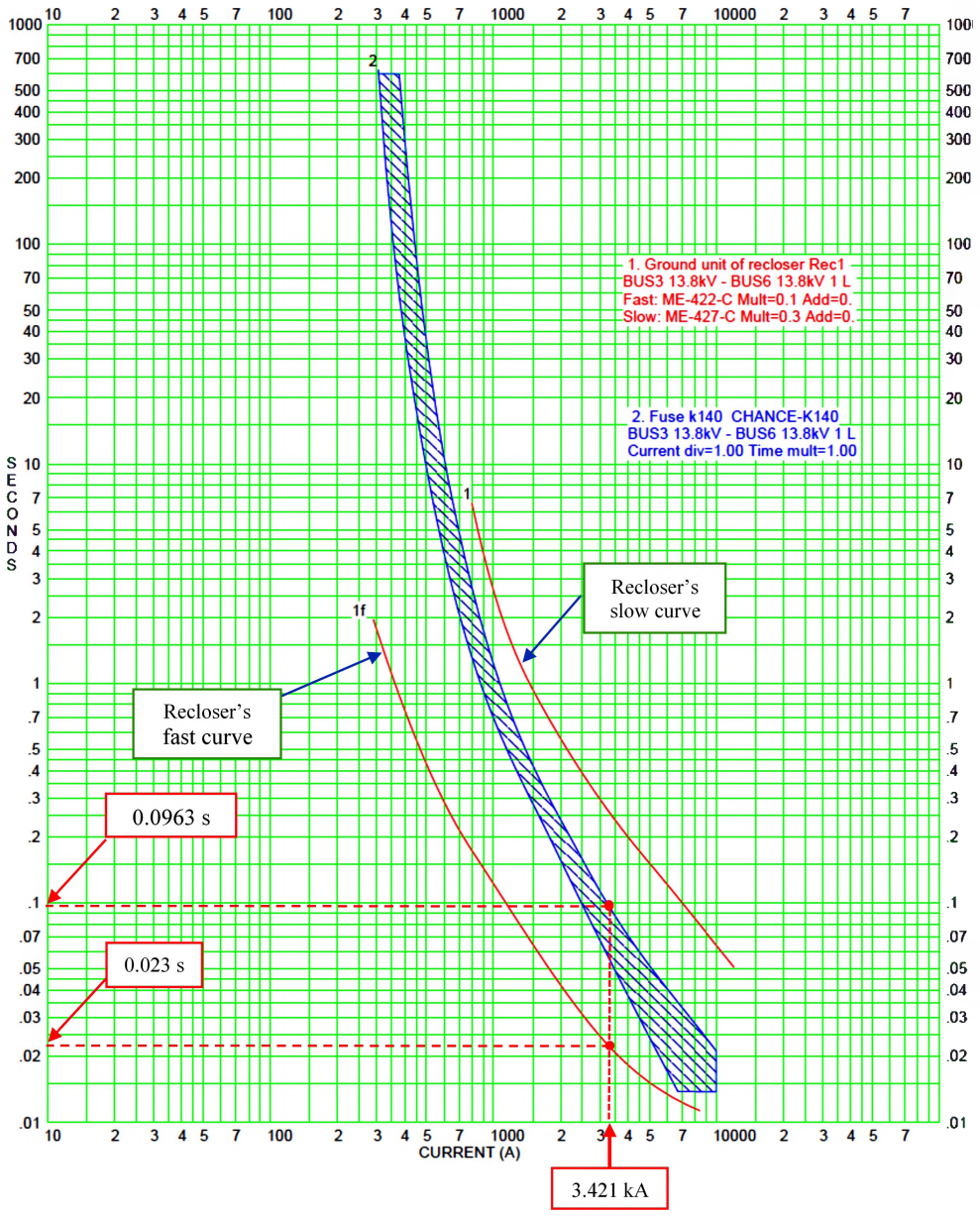

Figure 8. TCC for recloser-fuse coordination (case 1).

A. Therefore, the fuse-saving scheme saves the lateral fuse under temporary SLG fault and works as expected during the permanent SLG fault, which means that the set-up for the base system is valid, and different scenarios can be tested using this base system.

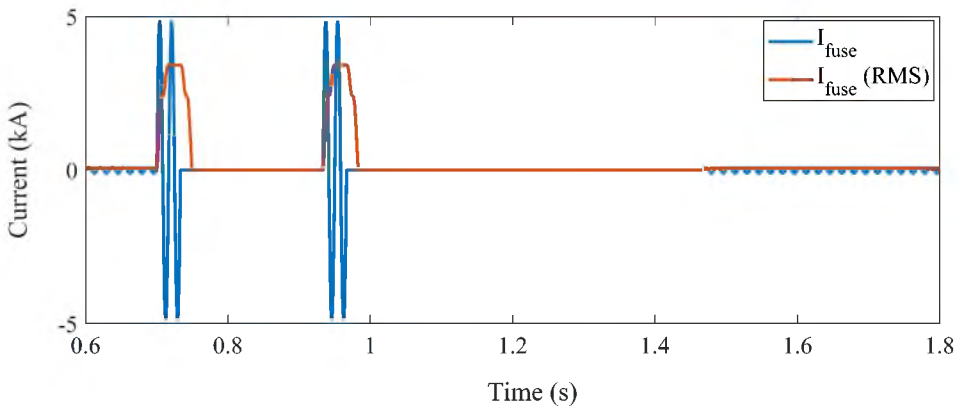

(a)

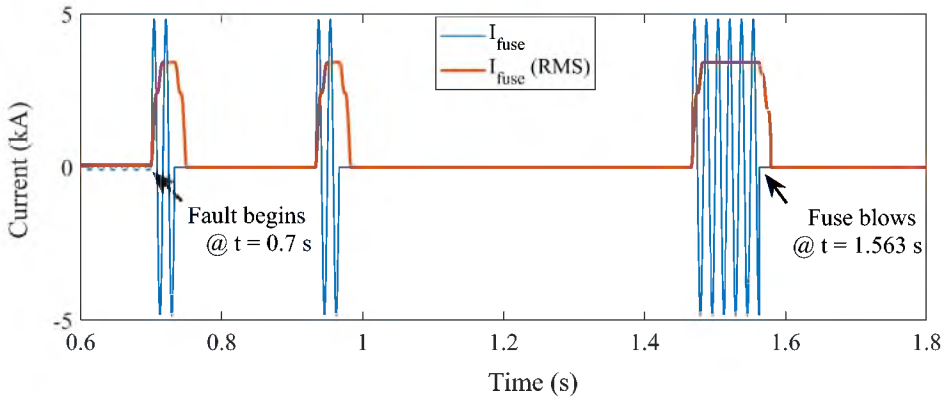

(b)

Figure 9. Simulated results of case 1: (a) Current magnitude for a temporary SLG fault and (b) Current magnitude for a permanent SLG fault.

3.2. CASE 2: BASE SYSTEM WITH IBDG

The system consists of a transformer that connects to the utility system and a radial network with a feeder that delivers the electric power to a resistive load through a lateral fuse. A utility-scale IBDG is connected to the feeder, as shown in Figure 10. A temporary SLG fault is applied at $t = 0.7\,s$ on the single-phase lateral. As a result, the fault current magnitude seen by the recloser on phase A is less than the fault current seen by the recloser with no IBDG (case 1) since the IBDG contributes to the fault current.

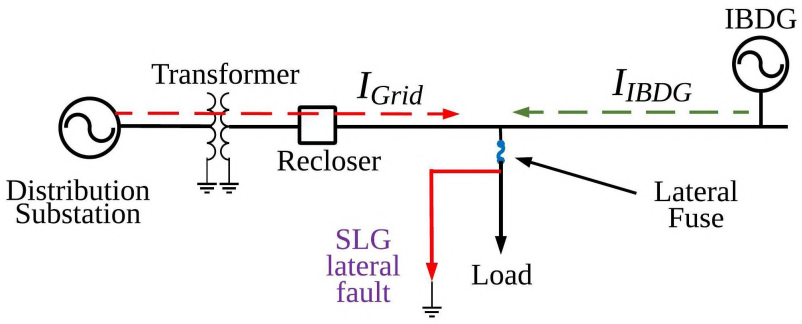

Figure 10. Single-phase test system diagram for case 2.

The fault current seen by the recloser on phase A exceeds the minimum setting for a ground pickup current; therefore, the recloser is supposed to perform its first fast operation at a time assigned by the TCC to save the lateral fuse. Despite that, the fuse melts and clears the temporary fault sooner than the first fast operation of the recloser due to the increase of fault current seen by the fuse after installing the IBDG. That means IBDG fault current contribution causes fail-to-trip of the recloser because the recloser sees a lower fault current. In other words, the sensitivity of the recloser is decreased and causes an erroneous operation. As a result, customers downline from the fuse on phase A will experience an unnecessary outage. Figure 11 shows the test result of case 2. It can be observed that the fault current magnitude passing through the fuse is the summation of both short-circuit currents from the IBDG and the substation. Therefore, compared to Case 1, due to the fault current increase after installing the IBDG, the fault is detected and isolated faster by the fuse. That means the recloser-fuse coordination does not work correctly due to the fault current contribution of IBDG.

3.3. CASE 3: BASE SYSTEM WITH IBDG AND THE PROPOSED METHOD

The system is similar to the one in case 2 and Figure 10 with the exception that this time we use the proposed method to control the current contribution of IBDG. The reference signal is selected to be 6 kHz in EM. A temporary SLG fault is applied at $t = 0.7\ s$

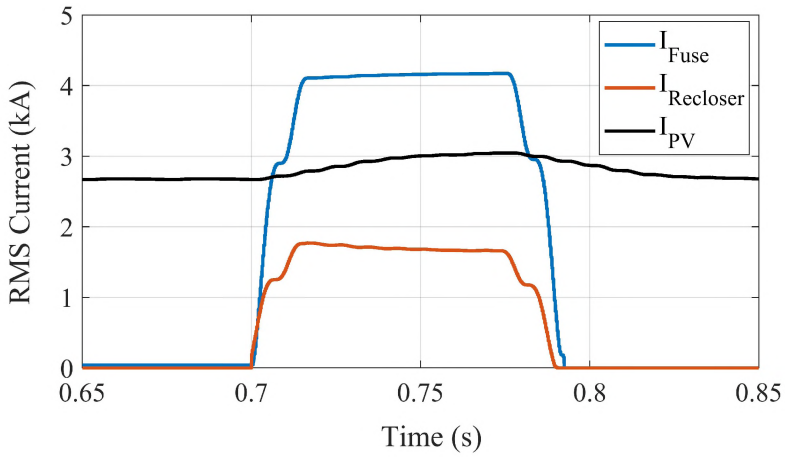

Figure 11. Simulated result for a temporary SLG fault (case 2): RMS current as seen by fuse, recloser, and IBDG.

on the single-phase lateral and self-cleared at $t = 1.2\,s$ (i.e., fault duration of 0.5 s). At the first 0.0167 s (1 cycle) of the fault, both the source and the IBDG feed the fault. At $t = 0.717\,s$ (0.0167 s or two cycles after the fault occurrence), the IBDG switched to 6 kHz (i.e., EM), and fault current contribution from IBDG goes to almost 0 A. At $t = 1.2\,s$, the fault is self-cleared, and the IBDG switched back to 60 Hz (i.e., NM) after two cycles once the recloser back online.

The dynamic of the system for EM is shown in Figure 12. When the fault occurs at $t = 0.7\,s$, it can be observed that the IBDG still generates about 1.3 times of its pre-fault current for one cycle, as shown in Figure 12a. At $t = 0.717\,s$, the EM activates, and the output current of the IBDG goes to almost zero A. In this mode, the fault current consists of the fault current contribution from the grid only. Once the fault self-cleared and the recloser back to supply loads, the IBDG switches back to NM (i.e., 60 Hz) in about two cycles.

Figure 12b-e illustrates the fuse and recloser status during a fault situation. Figure 12b shows that the fuse is intact; i.e., it is not blown. 0 in Figure 12b means that the fuse is still carrying the current, and 1 means the fuse is blown. Figure 12c shows the trip signal to the recloser, where 1 means the trip signal is sent to trip the CB, as shown in Figure 12e.

The control circuit of the recloser stays open during its first reclose interval, and once this interval expires, the close signal is sent to restore the recloser, as shown in Figure 12d. The recloser status corresponding to trip and close signals are shown in Figure 12e. These results demonstrate that implementing the proposed method with the IBDG maintains the fuse-saving scheme and saves the lateral fuse under a temporary SLG fault. The results of Cases 1-3 are summarized in Table 2.

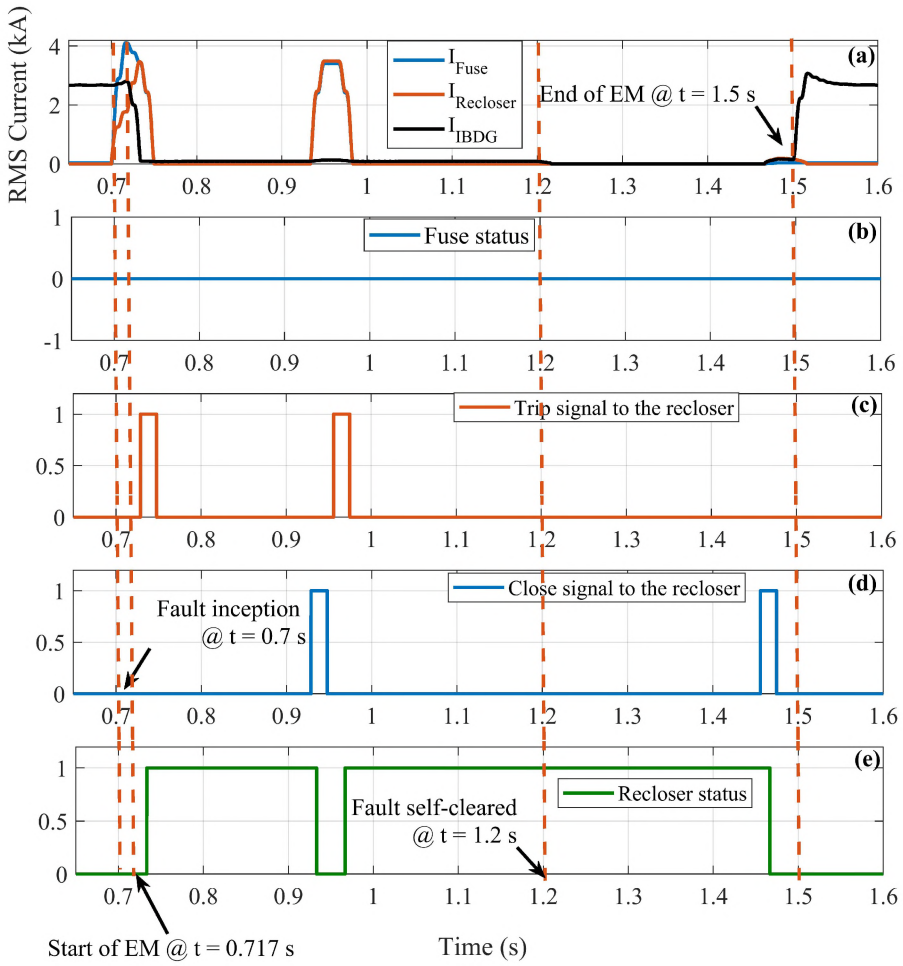

Figure 12. Simulated results for a temporary SLG fault (case 3): (a) RMS current as seen by fuse, recloser, and DG, (b) fuse status, (c) Trip signal to the recloser, (d) close signal from the control circuit to the recloser, and (e) recloser status.

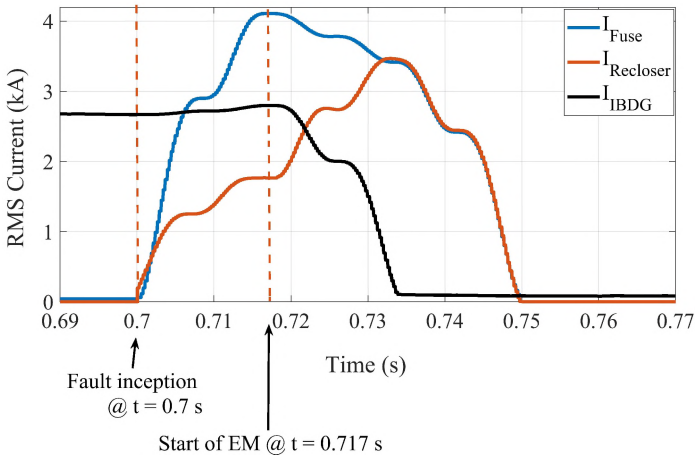

Figure 13. Zoomed in of the first part of Figure 12a.

Table 2. Summary of cases 1-3.

Cases	Results	Recloser	Fuse	Fuse-saving maintained?
Case 1: **Base Case**	Required	2 fast operations	Intact	Yes
	Simulation	2 fast operations	Intact	Yes
Case 2: **Base Case with IBDG Conventional Protection**	Required	2 fast operations	Intact	Yes
	Simulation	Failed to trip	Melted	No
Case 3: **Base system with IBDG and the proposed approach**	Required	2 fast operations	Intact	Yes
	Simulation	2 fast operations	Intact	Yes

Figure 14 shows the IBDG fault current contribution during fault for the same system at different EM frequencies. It can be observed that as the EM frequency decreases, the RMS fault current contribution of the IBDG during fault increases. Therefore, the fuse-saving scheme is no longer maintained.

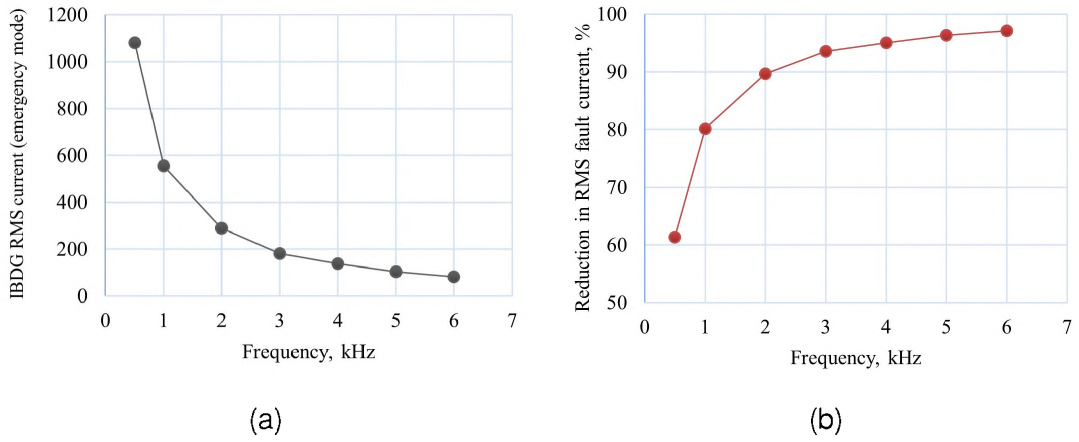

Figure 14. Emergency mode frequency vs.: (a) IBDG RMS current, and (b) the reduction in RMS fault current, %.

3.4. CASE 4: BASE SYSTEM WITH IBDG AND RESISTIVE SFCL

Figure 15 shows the network configuration. A resistive SFCL is integrated into the system to reduce the fault current contribution from the IBDG. The size of the resistive SFCL elements has been chosen to limit the fault current contribution from the IBDG to the same fault current magnitude generated by the IBDG during the emergency mode in case 3 (i.e., 81.8 A). The idea behind this is to compare the size of the inductor that interfaces the IBDG with the grid in the proposed method (i.e., case 3) against the current-limiting reactor's size of the resistive SFCL. Using the developed resistive SFCL model for this case, we observed that the required inductor size to reduce the fault current level to the same level as in case 3 (i.e., 81.8 A) is equal to 0.026 H. Thus, the size of the parallel inductor of the SFCL necessary to reduce the fault current contribution of the IBDG is approximately 100 times larger than the inductor size used to interface the IBDG into the distribution system ($L_{IBDG} = 0.25\,mH$). This case illustrated the inherent cost and size disadvantages of using a SFCL to limit fault current and how the proposed method can save money by keeping the size of the inductor small.

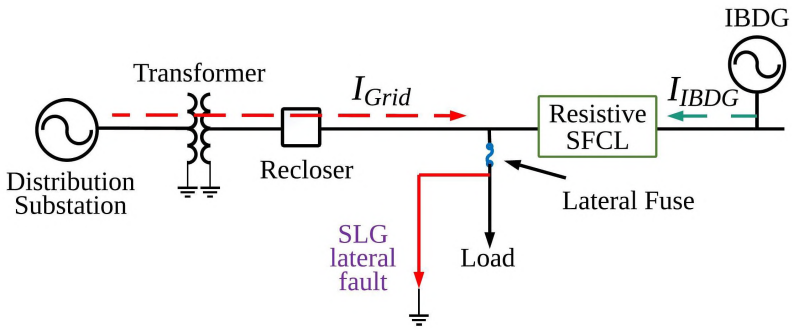

Figure 15. Single-phase test system diagram for case 4.

4. CONCLUSIONS

This paper proposes a novel approach to reduce the negative impact on protection coordination caused by integrating IBDGs on the distribution system by reducing the fault current contribution from IBDG under SLG fault conditions. It is shown that the current contribution of IBDG can be effectively limited using the embedded control of the IBDG that changes the frequency of the current, which in turn changes the inductor impedance used to interface the IBDG into the distribution system. This allows the conventional protection coordination scheme to be maintained without any additional cost of upgrading the network or adding more protecting devices. Furthermore, since the proposed method relies on existing components, it is inexpensive to implement.

BIBLIOGRAPHY

[1] T. Gonen, *Electric Power Distribution Engineering*, Third ed., Boca Raton: CRC Press, 2014, p. 769.

[2] N. Zhou, J. Wu and Q. Wang, "Three-phase short-circuit current calculation of power systems with high penetration of VSC-based renewable energy," *Energies (Basel)*, vol. 11, no. 3, p. 537, 2018.

[3] V. Gevorgian, M. Singh and E. Muljadi, "Symmetrical and unsymmetrical fault currents of a wind power plant," in *IEEE Power and Energy Society General Meeting*, San Diego, CA, USA , 2012.

[4] F. Xiao, Z. Zhang and X. Yin, "Fault Current Characteristics of the DFIG under Asymmetrical Fault Conditions," *Energies (Basel)*, vol. 8, no. 10, pp. 10971-10992, 2015.

[5] Hussain, B., Sharkh, S. M., Hussain, S. and Abusara, M. A., "An adaptive relaying scheme for fuse saving in distribution networks with distributed generation," *IEEE transactions on power delivery*, Vol. 28, no. 2, pp. 669-677, 2013.

[6] A. Y. Abdelaziz, H. E. Talaat, A. I. Nosseir and A. A. Hajjar, "An adaptive protection scheme for optimal coordination of overcurrent relays," *Electric Power Systems Research*, pp. 1-9, 2002.

[7] A. Elmitwally, E. Gouda, S. Eladawy, "Optimal allocation of fault current limiters for sustaining overcurrent relays coordination in a power system with distributed generation," *Alexandria Engineering Journal*, Vol. 54, no. 4, pp. 1077-1089, 2015.

[8] A. Elmitwally, E. Gouda and S. Eladawy, "Restoring recloser-fuse coordination by optimal fault current limiters planning in DG-integrated distribution systems," *International Journal of Electrical Power & Energy Systems*, vol. 77, pp. 9-18, 2016.

[9] A. LIM, J. KIM and J. KIM, "Study on Correction of Protective Devices for Application of a SFCL in a Power Distribution System With a Dispersed Generation," *IEEE Transactions on Applied Superconductivity*, vol. 23, no. 3, pp. 5603504-5603504, 2013.

[10] H. Jo, S. Joo and K. Lee, "Optimal Placement of Superconducting Fault Current Limiters (SFCLs) for Protection of an Electric Power System with Distributed Generations (DGs)," *IEEE Transactions on Applied Superconductivity*, vol. 23, no. 3, pp. 5600304-5600304, 2013.

[11] C.S. Shahriari, A. Yazdian and M. R. Haghifam, "Fault current limiter allocation and sizing in distribution system in presence of distributed generation," in *IEEE Power & Energy Society General Meeting*, Calgary, AB, Canada, 2009.

[12] W. El-Khattam and T. S. Sidhu, "Restoration of Directional Overcurrent Relay Coordination in Distributed Generation Systems Utilizing Fault Current Limiter," *IEEE Transactions on Power Delivery*, vol. 23, no. 2, pp. 576-585, 2008.

[13] H. H. Zeineldin and W. Xiao, "Optimal fault current limiter sizing for distribution systems with DG," in *IEEE Power and Energy Society General Meeting*, Detroit, MI, USA, 2011.

[14] L. K. Kumpulainen and K. T. Kauhaniemi, "Analysis of the impact of distributed generation on automatic reclosing," in *IEEE PES Power Systems Conference and Exposition*, New York, NY, USA, 2004.

[15] J. M. Gers and E. J. Holmes, *Protection of Electricity Distribution Networks,* London: IET, 2011, p. 107.

[16] F. A. Hariri, The Dynamic Behavior of a Solid State Transformer (SST) during Recloser Operation in Distribution Systems, Rolla, USA: ProQuest Dissertations Publishing, 2015.

[17] M. H. Bollen and F. Hassan, *Integration of Distributed Generation in Power System,* M. E. El-Hawary, Ed., Hoboken, New Jersey: John Wiley & Sons, 2011, p. 76.

[18] X. Tong and J. Liu, "Fault Processing Based on Local Intelligence," in *Fault Location and Service Restoration for Electrical Distribution Systems*, Singapore, John Wiley & Sons, 2016, pp. 9–72.

[19] S. Santoso, *Fundamentals of Electric Power Quality*, Winter 2012 ed. ed., Scotts Valley, CA: CreateSpace, 2012, p. 52.

[20] J. L. Blackburn and T. J. Domin, *Protective Relaying Principles and Applications*, Boca Raton, FL: CRC Press, 2014, p. 3.

[21] H. Zhan, C. Wang, Y. Wang, X. Yang, X. Zhang, C. Wu and Y. Chen, "Relay Protection Coordination Integrated Optimal Placement and Sizing of Distributed Generation Sources in Distribution Networks," *IEEE Transactions on Smart Grid*, vol. 7, no. 1, pp. 55-65, JANUARY 2016.

[22] M. E. Hamidi and R. M. Chabanloo, "Optimal Allocation of Distributed Generation With Optimal Sizing of Fault Current Limiter to Reduce the Impact on Distribution Networks Using NSGA-II," *IEEE Systems Journal*, vol. 13, no. 2, pp. 1714-1724, 2019.

[23] M. H. Rashid, *Power Electronics: Circuits, Devices, and Applications*, Third ed., Upper Saddle River, NJ: Pearson Education, 2004, p. 227.

[24] D. W. Hart, *Power Electronics*, International Edition ed., New York, NY: McGraw-Hill, 2011, p. 361.

[25] M. H. International, "PSCAD," Manitoba Hydro International Ltd. (MHI), [Online]. Available: https://www.pscad.com/. [Accessed 01 06 2021].

[26] "ASPEN OneLiner™," ASPEN, [Online]. Available: http://www.aspeninc.com/web/software/oneliner. [Accessed 01 06 2021].

III. MODELING AND SIMULATION OF RESISTIVE SUPERCONDUCTING FAULT CURRENT LIMITER IN PSCAD™/EMTDC™

Fahd A. Hariri, and Mariesa L. Crow
Department of Electrical & and Computer Engineering
Missouri University of Science and Technology
Rolla, Missouri 65409–0050
Email: fahrz9@mst.edu

ABSTRACT

Energy networks are facing significant challenges as the result of increasing electrical loads. To meet this rapid increase in demand for electricity, new generating units are being added to support the stability and reliability of the network. This change in network structure requires a comprehensive analysis of the effect of that increase on the protection system. Limiting the fault current to safe levels prevents replacing the high-cost network components that may be subjected to damage due to exceeding the rated short-circuit current values for which they were designed. A fault analysis often requires extensive modeling and simulation of the system, which requires accurate models of the protection system. This paper proposes a model for the resistive superconducting fault current limiter (SFCL) in PSCAD™/EMTDC™. The performance of the model is validated using a small test system.

Keywords: Resistive superconducting fault current limiter (SFCL), PSCAD™/EMTDC™, short-circuit current, protection system.

1. INTRODUCTION

The increasing demand for electrical energy has required the addition of generating capabilities to the electric power network. Usually, this demand is met by building new generating stations or expanding old ones as well as supporting the integration of distributed generators (DGs). All of these solutions must be studied in detail, particularly in terms of their impact on the protection system. In the event of faults, the short-circuit currents flow may be very high [1]. Network components are usually designed to tolerate fault currents for a short time period of up to one second, depending on the expected magnitude of the fault current. The high magnitude of a fault current with a long duration can damage network components, including cables, transformers, circuit-breakers (CBs), etc.

Fault current limiters (FCLs) are one of the approaches that have been used for decades in power systems to limit fault currents. The FCL is a device with a variable impedance. Under normal conditions, it presents a negligible reactance and dissipates very little energy. However, during the fault conditions, the FCL increases its reactance to limit the short-circuit currents significantly. Adding more renewable energy resources to the system frequently increases the short-circuit current level, which requires upgrading the system components to prevent potential failures. FCLs can mitigate this issue by limiting fault currents without upgrading the system components. The FCL can be added in series to an existing network without making any other configuration changes. However, a permanently inserted current-limiting series reactor introduces additional losses and can lead to power quality issues [2].

The process of triggering FCLs by fault currents is illustrated in Figure 1. The FCL limits the fault current by increasing its reactance if the fault current goes beyond its pre-determined threshold. Therefore, the short-circuit current is limited, which provides the circuit breaker (CB) a longer period in which to react.

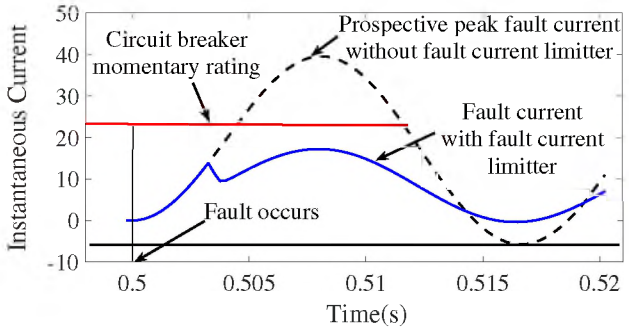

Figure 1. Time current profile with application of FCL.

A resistive superconducting fault current limiter (SFCL), which is explained in Section 2, is a type of FCL that may be used in a power system. Thus, the need for a reliable and accurate model of a resistive SFCL is important for protection studies. Therefore, the objective of this paper is to model a resistive-SFCL with a parallel current-limiting reactor. Simulation studies on this paper have been conducted using the PSCAD™/EMTDC™ software [3]. A resistive-SFCL model is not currently available in the PSCAD™/EMTDC™ libraries and thus this paper bridge this gap by proposing a resistive model of SFCL in PSCAD™/EMTDC™ software.

This paper is structured as follows: A background on FCLs is reviewed in Section 2, followed by a theoretical analysis of modeling the resistive SFCL. A description of the designed resistive SFCL model is presented in Section 3. Then, in Section 4, the proposed model is validated via multiple case studies. Finally, Section 5 concludes the paper.

2. TYPES OF FAULT CURRENT LIMITERS

A plethora of research has been proposed to control and limit fault currents using FCLs in transmission and distribution systems embedded with DGs. FCLs can be classified as solid-state FCLs, passive FCLs, and hybrid FCLs (i.e., combination of solid-state and passive FCLs devices) [4]. Passive FCLs, which are also called self-controlled FCLs, have

a simple structure, usually consisting of series reactors or resistors. On the other hand, the solid-state FCLs need an external control circuit using a fault detection algorithm to control the power electronics equipment to limit the short-circuit current.

A solid-state FCL is usually comprised of an over-current detector, a control device, and a fast power electronics switch in series with the voltage source or DG, to limit the sudden overvoltage that appears across the switch caused by the sudden interruption of fault current. Under normal system conditions, the solid-state switch carries the normal current. When the fault occurs, the fault detection circuit senses the rising fault current and sends a turn-off signal to the switch. Thus, the fault current is diverted to the current limiting impedance. Solid-state FCLs have higher accuracy than the passive FCLs but also have a higher cost and suffer from continuous conduction losses [2].

A superconducting fault current limiter (SFCL) is a type of FCL that may be used in a power system. Improving the performance of these devices is an active avenue of research [5]. There are four types of SFCLs [2]: shielded inductance SFCL, saturated inductance SFCL, air-gap SFCL, and resistive SFCL. The resistive SFCL is mainly composed of a wire, or a coil, such that its non-linear characteristics controls the behavior of its superconducting materials, such as Bismuth-2233 or $YBa_2Cu_3O_7$, to current, magnetic fields, temperature. The resistance of the superconductor goes to zero during the superconductivity state which takes place at temperatures of -270°C to -273°C [2]. Under normal conditions, the superconductor acts as a near-perfect conductor. When the fault occurs, the current passing through the superconductor becomes greater than the material's critical value, which makes the superconductor highly resistive. The SFCL has many disadvantages, such as a high cooling cost, a large footprint, and a CB is required in the case of a permanent fault. Furthermore it can limit only about one-third of the prospective fault currents [6].

The impedance value of the FCL under fault conditions determines the size and cost of the FCL. Therefore, as the size increases, the FCL cost increases [7]. Optimal locations, sizes, and numbers of FCLs in the radial distribution systems in the presence of DG are discussed in [8], [9].

2.1. THEORETICAL ANALYSIS

Figure 2 shows a resistive SFCL with a parallel current limiting reactor. Under normal conditions (Figure 2(a)), the superconductor has a zero resistance. However, the fault current is shared between the parallel current limiting reactor and the superconductor during a fault (Figure 2(b)). This method rapidly helps the cooling and recovery of the superconductor (about 1-2 msec) instead of several minutes, which means that a fast reclosing operation can be achieved. We leveraged the mathematical model for SFCL in [10] to build the PSCAD™/EMTDC™ model for SFCL. For ease of understanding, the mathematical model for SFCL [10] are represented in (1)–(29).

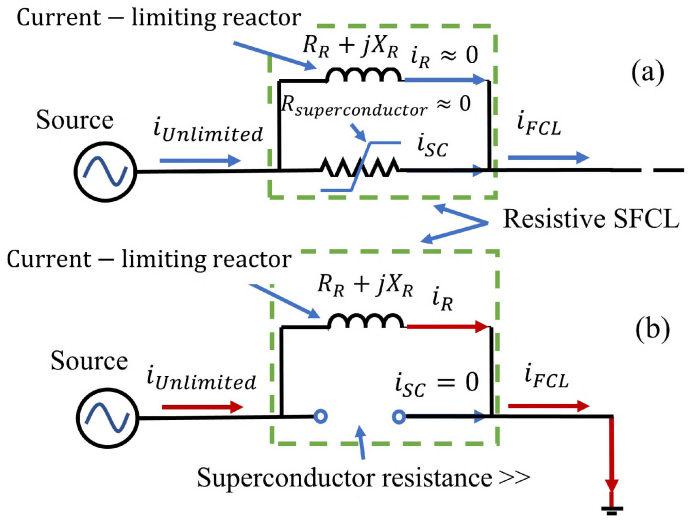

Figure 2. (a) System operation under normal condition where the resistance of the resistive SFCL ≈ 0, and (b) System operation under normal condition where the resistance of the resistive SFCL is very high.

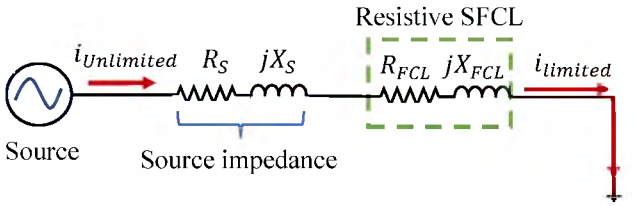

Figure 3. Series resistive SFCL representation.

Referring to Figure 2, the leakage impedance of the parallel current limiting reactor can be written as

$$Z_R = R_R + j\omega L_R \tag{1}$$

Figure 3 shows the equivalent impedance of the SFCL which can be expressed as

$$Z_{FCL} = R_{FCL} + jX_{FCL} \tag{2}$$

$$= \frac{R_{SC}[X_R^2 + R_R(R_{SC} + R_R)]}{(R_{SC} + R_R)^2 + X_R^2} + j\frac{R_{SC}^2 X_R}{(R_{SC} + R_R)^2 + X_R^2} \tag{3}$$

where R_{FCL} and X_{FCL} are the equivalent resistance and reactance of the SFCL, respectively. R_{SC} is the quenched superconductor resistance. Neglecting the resistance of the reactor yields

$$Z_{FCL} = \frac{R_{SC}X_R^2}{R_{SC}^2 + X_R^2} + j\frac{R_{SC}^2 X_R}{R_{SC}^2 + X_R^2} \tag{4}$$

In practical designs and during fault conditions, R_{SC} is larger than X_R. Thus, substituting $R_{SC} = kX_R$ into (4) yields,

$$R_{FCL} = \frac{k}{k^2 + 1}X_R \tag{5}$$

$$X_{FCL} = \frac{k^2}{k^2 + 1}X_R = kR_{FCL} \tag{6}$$

where

$$k = \frac{R_{SC}}{X_R} = \frac{X_{FCL}}{R_{FCL}} \tag{7}$$

To reduce the symmetrical RMS or initial peak fault current, the value of X_R should be selected in a cost-effective manner to achieve the required reduction. Usually, that reduction can be in a range of 40% to 80% [10]. From Figure 3, the unlimited and limited fault currents are given by

$$I_{Unlimited} = \frac{V_S}{R_S + jX_S} \tag{8}$$

$$I_{Limited} = \frac{V_S}{(R_S + jX_S) + (R_{FCL} + jX_{FCL})} \tag{9}$$

and

$$m = \left| \frac{I_{Unlimited} - I_{Limited}}{I_{Unlimited}} \right| \tag{10}$$

where m is the reduction in symmetrical RMS fault current. Substituting (7), (8) and (9) into (10) and solving for R_{FCL}, gives

$$R_{FCL} = \frac{m^2(R_S + kX_S) + A}{BC} \tag{11}$$

where

$$A = m\sqrt{m^2(R_S + kX_S)^2 + BC(R_S^2 + X_S^2)} \tag{12}$$

$$B = 1 - m^2 \tag{13}$$

$$C = 1 + k^2 \tag{14}$$

Let the voltage source behind the source impedance $R_S + j\omega L_S$ in Figure 2a be

$$v_S(t) = \sqrt{2}V_{rms}\sin(\omega t + \theta) \tag{15}$$

Therefore, the unlimited short-circuit current is given by

$$i_S(t) = \frac{\sqrt{2}V_{rms}}{Z_S}\left[\sin\left(\omega t+\theta-\tan^{-1}\left(\frac{X_S}{R_S}\right)\right) - \sin\left(\theta-\tan^{-1}\left(\frac{X_S}{R_S}\right)\right)e^{\frac{-t}{\frac{L_S}{R_S}}}\right] \quad (16)$$

where

$$X_S = \omega L_S \quad (17)$$

$$Z_S = \sqrt{R_S^2 + X_S^2} \quad (18)$$

Similarly, the limited short-circuit current is given by

$$i_{FCL}(t) = \frac{\sqrt{2}V_{rms}}{Z_E}\left[\sin\left(\omega t+\theta-\tan^{-1}\left(\frac{X_E}{R_E}\right)\right) - \sin\left(\theta-\tan^{-1}\left(\frac{X_E}{R_E}\right)\right)e^{\frac{-t}{\frac{L_E}{R_E}}}\right] \quad (19)$$

where

$$R_E = R_S + R_{FCL} \quad (20)$$

$$L_E = L_S + L_{FCL} \quad (21)$$

$$X_E = X_S + X_{FCL} \quad (22)$$

The currents flowing through each branch of the resistive SFCL are

$$i_{FCL}(t) = i_{SC}(t) + i_R(t) \quad (23)$$

$$R_{SC}i_{SC}(t) = L_R\frac{di_R(t)}{dt} \quad (24)$$

$$v_S(t) = R_S i_{FCL}(t) + L_S\frac{di_{FCL}(t)}{dt} + R_{SC}i_{SC}(t) \quad (25)$$

From (19) and (25), the current flowing through R_{SC} is given by

$$i_{SC}(t) = \frac{\sqrt{2}V_{rms}}{Z_E R_{SC}} \left[\sqrt{Z_E^2 + Z_S^2 - 2Z_E Z_S \cos(\beta)} \times \sin\left(\omega t + \theta - \tan^{-1}\left(\frac{Z_S \sin(\beta)}{Z_E - Z_S \cos(\beta)}\right)\right) + \left(R_S - \frac{X_S}{X_E} R_E\right) \sin\left(\theta - \tan^{-1}\left(\frac{X_E}{R_E}\right)\right) e^{\frac{-t}{\frac{L_E}{R_E}}} \right] \quad (26)$$

where

$$X_E = \omega L_E \quad (27)$$

$$Z_E = \sqrt{R_E^2 + X_E^2} \quad (28)$$

$$\beta = \tan^{-1}\left(\frac{X_S}{R_S}\right) - \tan^{-1}\left(\frac{X_E}{R_E}\right) \quad (29)$$

From (19) and (26), the current flowing through L_R can be written as

$$i_R(t) = i_{FCL} - i_{SC}(t) \quad (30)$$

3. RESISTIVE SFCL MODEL IN PSCAD™/EMTDC™

The main components of the proposed resistive SFCL model are the current limiter connected in parallel with a circuit breaker and an external control unit, as shown in Figure 4. We have proposed a novel control scheme for controlling the SFCL status via opening and closing the CB in Figure 4. Note that the CB in Figure 4 is not an actual circuit breaker in the system. However, it is used in the model to mimic the transition between two states (i.e., operates as a switch) of the SFCL.

The current limiter consists of two elements: a current-limiting reactor and a quenched superconductor element. For the short-circuit analysis, a fixed-resistance can be used to represent the latter [10]. Under normal operating conditions, the current flows

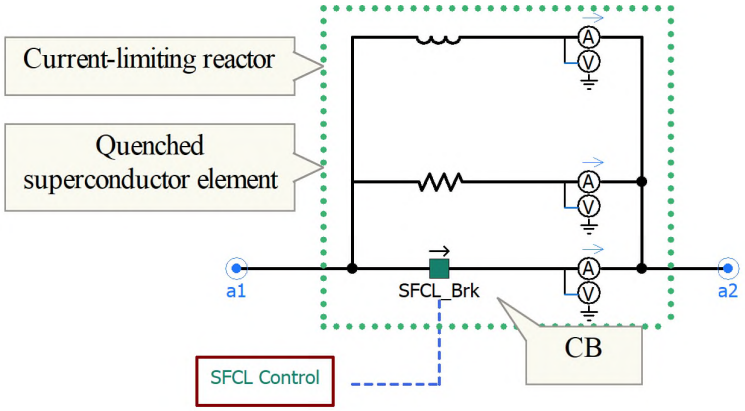

Figure 4. Resistive SFCL model in PSCAD™/EMTDC™.

through the CB. When a fault occurs, the current increases and the CB opens to divert the fault current through the resistor and reactor. The transition in the breaker state from closed (superconductivity state) to open (high resistive state) mimics the loss of the superconducting state of the resistive SFCL during the short-circuit. The resistor represents the increase of the superconductor resistance, which quenches the fault current. Thus, due to the high value of the quenched superconductor resistor, the reactor becomes the easiest path for most of the fault current to pass through.

The block diagram of the control unit is shown in Figure 5. The function of the control unit is to control the CB operation and it consists of the SFCL quench logic and the SFCL recovery logic. In order for the SFCL quench logic to operate and send the trip signal to the CB, two conditions must be met: the high increase in the current magnitude and the rate of the current rise. Thus, the SFCL quench logic starts with measuring the magnitude of the current passing through the resistive SFCL. If the measured current I_S is higher than the threshold (i.e., current setting) $I_{setting}$, then the output of the "Over Current Detection" block acquires the value of 1 and stays on this level.

The "Monostable" block, in Figure 5, receives the output of the "Over Current Detection" block and changes it into a pulse. At the same time, the two input comparator components determine if the rate of rise of the fault current $\frac{di}{dt}$ is increasing above the

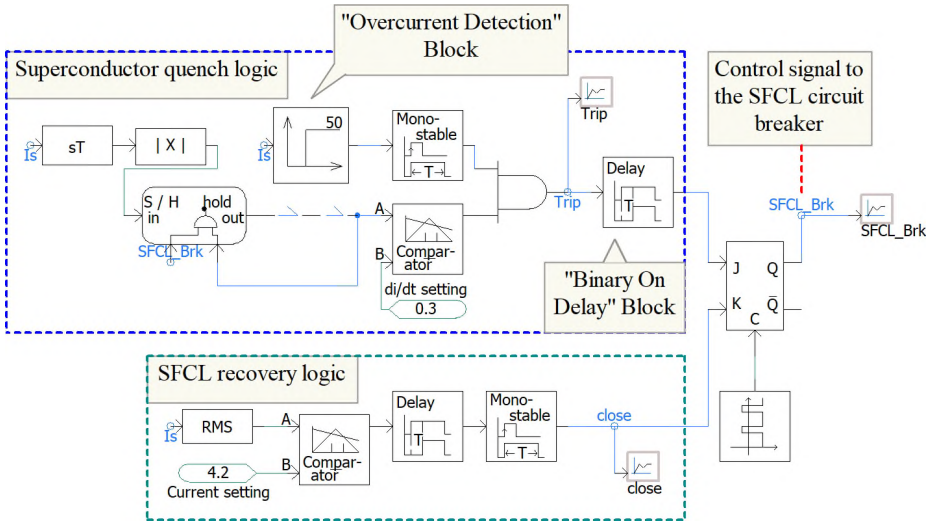

Figure 5. Resistive SFCL control model in PSCAD™/EMTDC™.

$(\frac{di}{dt})_{setting}$. If these two conditions are met (i.e., the high increase in both the current magnitude and the rate of current rise), then this indicates the existence of a fault condition somewhere in the system and a trip signal will be sent to the CB. The trip signal will be delayed by a "Binary On Delay" block for a specified time before sending it to the CB. The delay time is typically 1-2 ms, which represents the time required by the resistive SFCL to transition to a high resistive state [10].

To initiate the SFCL recovery logic, the measured RMS current value should be less than the current setting value. Once this condition is met, the output of the comparator element will be 1. The close signal will wait for a time period dictated by the design of the protection scheme. This time delay, which is usually a few seconds, represents the time needed by the superconductor element to cool down and recover [10]. The output of the "Binary On Delay" block is fed into the monostable block to change the constant signal into a pulse close signal.

To control the operation of the CB in this model, both the trip and close signal are fed into the "J-K flip-flop" block. Details of the flip-flop and its control of the circuit breaker are in [11]. The flowchart of the proposed SFCL model is shown in Figure 6.

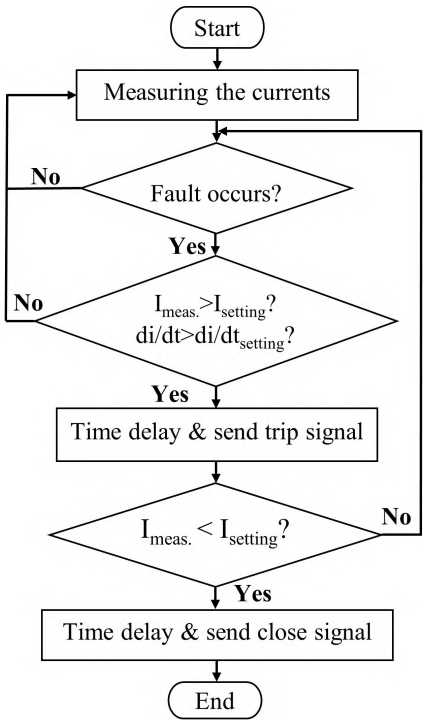

Figure 6. Flowchart of the proposed SFCL model.

4. MODEL VALIDATION

To authenticate the functionality of the proposed resistive SFCL model, it is deployed on a simple three-phase radial system. Figure 7 shows the test system that is built in PSCAD™/EMTDC™ to study the performance of the SFCL model. The system consists of a voltage source connected to a load through a resistive-SFCL. It is required to reduce the fault current from 15 kA-RMS to 6 kA-RMS, which equivalent to an approximate 60% reduction. Parameter values of the test system are given in Table 1. Three three-phase line-ground (3LG) fault cases have been considered:

- Case 1: Permanent 3LG fault at $t = 0.5\ s$.
- Case 2: Temporary 3LG fault at $t = 0.5\ s$ and at $t = 4\ s$.
- Case 3: Temporary 3LG fault at $t = 0.5\ s$ and at $t = 2\ s$.

The fault duration in each case is 1 second, the recovery interval is 2 seconds, and the fault resistance is zero ohms.

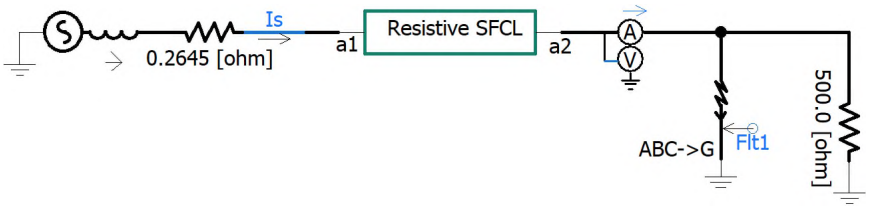

Figure 7. One-line diagram of the test system in PSCAD™/EMTDC™.

Table 1. Parameter values of the test system

Parameters	**Value**
Line–line Input voltage (utility's source)	138 kV-rms
Power frequency	60 Hz
Fault Nature	3LG solid fault
Symmetrical RMS short-circuit current	15.06 kA
X/R ratio of the system, $\frac{X_S}{R_S}$	20
The desired limited fault current (in RMS)	6 kA
Resistive SFCL trigger current	2 kA instantaneous
$k = \frac{R_{SC}}{X_R}$	6

The 3LG bolted fault is not as common as the other types of faults such as line-to-line-to-ground (LLG) faults or line-to-ground (LG) faults, but it is purposely considered in this paper because the maximum short-circuit current is seen in the case of 3LG fault, and it is used in the interruption selection and equipment current withstanding capabilities [1]. Thus, a SFCL designed for the 3LG bolted faults can protect the power system components from being damaged in LG or LLG bolted faults as well. A MATLAB script is written to compute the required parameters and to plot the current waveforms based on the equations in Subsection 2.1 and the given system data in Table 1. The output of the MATLAB script which are the required parameters for the simulation are tabulated in Table 2.

Table 2. Calculated values of the test system parameters

Parameters	Z_S	R_S	X_S	X_R	R_{SC}
Value	5.29 Ω	0.2645 Ω	5.2834 Ω	8.067 Ω	48.402 Ω

4.1. CASE 1: PERMANENT 3LG FAULT OCCURS AT t = 0.5 s

In order to test the operation of the SFCL model under fault conditions, a permanent symmetrical fault (i.e., 3LG fault) is applied between the SFCL and the load at $t = 0.5\,s$. Figure 8 shows the output from the PSCAD™/EMTDC™ simulation. At the moment of the 3LG fault at $t = 0.5\,s$, it can be observed that the fault current magnitude without SFCL, shown by the blue color, is increased to 19.85 kA-RMS during the first half cycle (i.e., subtransient period) and then is decreased to 15.06 kA-RMS during the steady-state period. At the same time, we can observe the impact of the SFCL model implementation on the fault current magnitude during the same fault period which is shown by red color in Figure 8. We can note that the current magnitude with SFCL reaches the value of 10.77 kA-RMS during the first half cycle and then decreases to about 6 kA-RMS during the steady-state period. It can be observed from the simulation result that the RMS fault current is decreased as required from 15 kA-RMS to 6 kA-RMS.

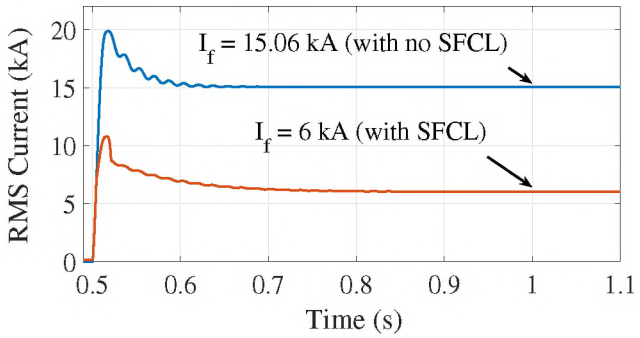

Figure 8. Simulated performance of the SFCL (case 1).

4.2. CASE 2: TEMPORARY 3LG FAULT AT t = 0.5 s AND AT t = 4 s

This case simulates the impact of the proposed SFLC model on limiting the short-circuit current for recurring temporary faults. Figure 9 shows the expected behavior of the fault current during different statuses of the SFCL model. In this case, a 3LG fault is imposed at t_0 and is cleared at t_2. At t_0, the current increases to its maximum value before

the transition of the SFCL from superconductivity-state to the high-resistive state at t_1. The fault current will be limited during the high resistive-state which lasts until the end of the fault duration at t_2. The CB of the SFCL model will remain open until the recovery interval expires at t_3. After t_3, the SFCL will return to its superconductivity-state by closing its CB. A 3LG fault occurs again at t_4 and self-cleared at t_6. The CB closes at t_7 to announce the end of the recovery interval. The expected maximum and steady-state current magnitude are similar to the fault that occurs at t_0. That is because the second fault at t_4 occurred during the time when the SFCL is in its superconductivity-state. Figure 9 shows the expected current profile of the SFCL in case 2.

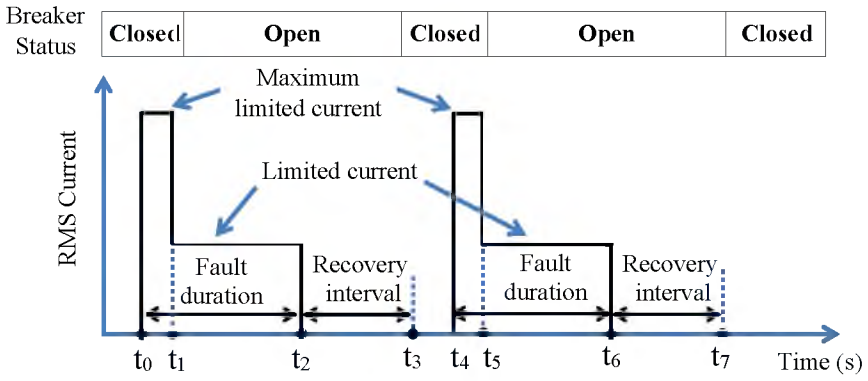

Where:

t_0, t_4: Starting time of the fault.

t_1, t_5: Transition time of the SFCL from superconductivity-state to high-resistive state.

t_2, t_6: End time of the fault.

t_3, t_7: End time of the recovery interval.

Figure 9. Expected performance of the SFCL (Case 2).

Similarly, Figure 10 shows the simulation results for the proposed SFCL model. During the first fault interval, it can be observed that the current magnitude reaches the value of 20 kA-RMS then decreases to 15 kA-RMS during the following steady-state cycles. The same current profile can be noticed during the second fault interval because the second fault occurred at the time when the SFCL is at it's superconductivity-state.

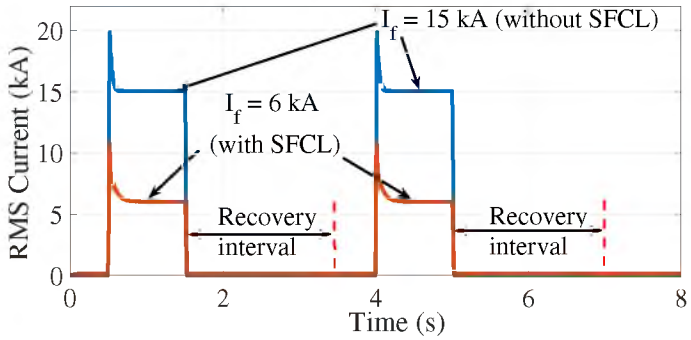

Figure 10. Simulated performance of the SFCL (case 2).

4.3. CASE 3: TEMPORARY 3LG FAULT AT t = 0.5 s AND AT t = 2 s

In order to further validate the performance of the proposed SFCL model, two consecutive temporary faults are utilized in which the second fault occurs before the SFCL has fully recovered. According to the recovery logic, the SFCL should stay at a high-resistive state until the end of the recovery interval. Therefore, if a fault occurs during that recovery interval, the fault current will be limited directly without any time delay because the SFCL still is in a high-resistive state. This means the current magnitude will not reach the magnitude when the fault occurred at $t = 0.5\ s$ because the transition moment does not exist in this case.

A temporary symmetrical fault has been applied between the SFCL and the load at $t = 0.5\ s$. The fault is self-cleared at $t = 1.5\ s$ and another symmetrical fault occurs during the recovery interval at $t = 2\ s$. Figure 11 shows the output from the PSCAD™/EMTDC™ simulation. At the moment of the first 3LG fault, it can be observed that the current magnitude increases up to 10.77 kA-RMS during the first half cycle (i.e., subtransient period) and then decreases to 6 kA-RMS during the steady-state period. At the time of occurring the second fault, we can observe that the maximum fault current magnitude is 8.2 kA-RMS which is less than 10.77 kA-RMS, for the first fault, because the SFCL still at its a high-resistive state.

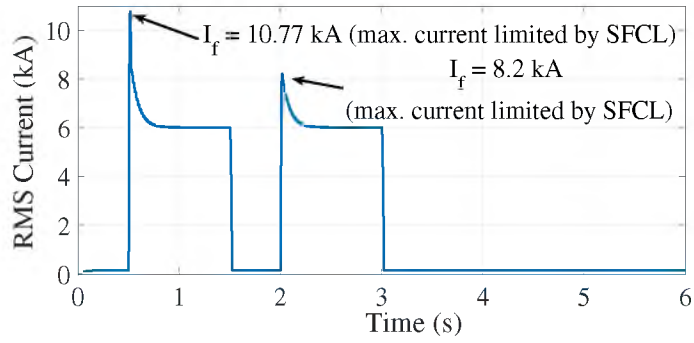

Figure 11. Simulated performance of the SFCL (case 3).

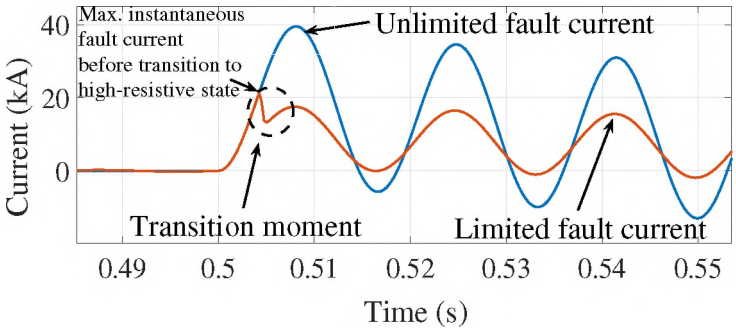

Figure 12. Transition moment of the SFCL (case 3).

The transition moment of the SFCL from the superconductivity-state to high-resistive state is shown in Figure 12. It can be observed from the simulation results that the RMS fault current passing through the SFCL is decreased as the SFCL control scheme designed for.

5. CONCLUSIONS

A new control scheme for the resistive-SFCL is successfully modeled and analyzed in PSCAD™/EMTDC™. The implementation of the SFCL in the test system under both permanent and temporary faults showed that the resistive SFCL model operated as designed. The control circuit of the SFCL performed its tasks appropriately by controlling the CB operations. All settings and values of the model components can be adjusted to suit the

requirements of the underlying test system. Therefore, this model can be easily implemented in electrical networks to further investigate the impacts of this type of fault current limiter on the protection schemes.

BIBLIOGRAPHY

[1] "Recommended practice for calculating ac short-circuit currents in industrial and commercial power systems," *IEEE Std 551-2006 [TheViolet Book]*, pp. 1–308, 2006.

[2] N. Tleis, *Power Systems Modelling and Fault Analysis-Theory and Practice*, Elsevier, 2007, ch. Permanently inserted current limiting series reactor, [Online]. Available: http://ebookcentral.proquest.com/lib/umrebooks/detail.action?docID=319163.

[3] M. H. International, "PSCAD version 5.0," Manitoba Hydro International Ltd. (MHI), [Online], Available: https://www.pscad.com/. [Accessed 01 06 2021].

[4] T. Ghanbari and E. Farjah, "Development of an efficient solid-state fault current limiter for microgrid," *IEEE Transactions on Power Delivery*, vol. 27, no. 4, pp. 1829–1834, 2012.

[5] J. Das, *Short-Circuits in AC and DC Systems: ANSI, IEEE, and IEC Standards*, CRC Press, 2017, ch. Short-circuit calculations according to ANSI standards.

[6] M. M. R. Ahmed, "Development of a solid-state fault current limiting and interrupting device suitable for power distribution networks," Ph.D.dissertation, Northumbria University, 2002.

[7] A. Elmitwally, E. Gouda, and S. Eladawy, "Optimal allocation of faultcurrent limiters for sustaining overcurrent relays coordination in a power system with distributed generation," *Alexandria Engineering Journal*, vol. 54, no. 4, pp. 1077–1089, 2015.

[8] S. Shahriari, A. Yazdian and M. Haghifam, "Fault current limiter allocation and sizing in distribution system in presence of distributed generation," *2009 IEEE Power & Energy Society General Meeting*, 2009, pp. 1-6, doi: 10.1109/PES.2009.5275298.

[9] H. H. Zeineldin and W. Xiao, "Optimal fault current limiter sizing for distribution systems with DG," *2011 IEEE Power and Energy Society General Meeting*, 2011, pp. 1-5, doi: 10.1109/PES.2011.6038967.

[10] N. Tleis, *Power Systems Modelling and Fault Analysis-Theory and Practice*, 2nd ed., Elsevier, 2019, ch.10.5.2 Modelling of Resistive Superconducting Fault Current Limiters for Short-Circuit Analysis,[Online], Available:https://app.knovel.com/hotlink/khtml/id:kt0122V9V5/power-systems-modelling/modelling-resistive-superconducting

[11] F. A. Hariri, The Dynamic Behavior of a Solid State Transformer (SST) during Recloser Operation in Distribution Systems, Rolla, USA: ProQuest Dissertations Publishing, 2015.

SECTION

2. CONCLUSION

This dissertation aimed to find innovative solutions to upgrade the protection systems for modern distribution networks. The proposed solutions were presented in three papers. In Paper I, the impact of infeed effect caused by DGs was solved by three different new methods. Each method uniquely addressed the issue. However, all proposed methods depended only on local measurements. In Paper II, the fuse-saving scheme was maintained by a novel approach to reduce the negative impact of integrating IBDGs with the distribution system protection scheme. The proposed approach controlled the IBDG to reduce the fault current contribution from IBDG under SLG fault conditions. Finally, in Paper III, a new control scheme for the resistive-SFCL was successfully modeled. This new control scheme for resistive-SFCL was successfully tested under different fault conditions. The performance of the proposed methods in this dissertation was demonstrated with radial distribution system models in PSCAD™/EMTDC™.

VITA

Fahd Amin Hariri received his bachelor of science (B.S.) in Electrical Engineering from the King Abdulaziz University, Jeddah, Saudi Arabia, in December 2004. From 2005 to 2009, he was a transmission engineer at Saudi Electricity Company, Jeddah, Saudi Arabia. Since 2009, he was a teaching assistant in the Electrical Engineering Department at the King Abdulaziz University. He received his Master's of Science (M.Sc.) in Electrical Engineering from Missouri University of Science and Technology, Rolla, Missouri in July 2015. He received his Ph.D. in Electrical Engineering from Missouri University of Science and Technology, Rolla, Missouri in July 2021. His research interests included power systems and power systems protection.